MEASUREMENT OF POWER IN RESEARCH REACTORS USING THE NEUTRON NOISE TECHNIQUE

A. GOMEZ, R. WALDMAN+, E. LAGGIARD

ABSTRACT

A high precision method based on the neutron noise technique in the frequency domain is proposed to measure the stationary power in a research reactor. An expression of the Power Spectral Density (PSD) was obtained using a theoretical modal solution for the detector field of view. The measured PSD data was fitted using the first term of the solution. The principal theoretical hyphotesis verified experimentally was the predominance of both the fission density fluctuation as the correlated source of noise and the fundamental adjoint kinetic eigenfunction in the detectors' field of view.

Measurements were made in natural and forced convection in the RA-6 research reactor located at the Centro Atómico Bariloche (CAB), Argentina, in different critical arrangements.

For practical purposes it was found that the method can be applied between 10 w and 50 Kw and it does not depend on detector locations. The method was used to calibrate other~~s~~ relative methods in order to measure higher power. The measurements agree with the results obtained using a calorimetric method.

I. INTRODUCTION

One of the more important measurements in reactor physics is the determination of the absolute thermal power of a nuclear reactor. For low power, natural convection reactors, this quantity is usually obtained by absolute counting, foil activation or statistical methods. For forced convection reactors the higher power is also determined by calorimetric or N^{16}-gamma counting methods.

The principal characteristics of each method are the following:

The absolute counting method uses neutron detectors such as ionization or fission chambers, BF_3 or He^3 counters. Since the output from these detectors is proportional to the nearby flux it is not possible to obtain the total fission rate. Usually it is necessary a calibration process (the relation between the power and the measured output) but this process could be affected by changes in the core arrangement, for example, control-rods movements or different reflector materials.

The foil activation method involves an integration of a detection reaction rates over the core volume and the absolute activation measurements in some points in the reactor. It is time expensive and needs corrections due to flux depression and shielding associated with foils. The sources of error are the inacurate knowledge of the neutron spectrum and the cross sections, the hyphotesis used to interpolate the flux in positions near control rods and in the calibration process to obtain the absolute detector efficiency.

The calorimetric method can be easily applied provided most of the primary circuit flow passes throughout the core. The main error sources are: the small difference in the inlet-outlet coolant temperature and the uncertainty in the effective coolant flow value. Usually this method is suitable for forced convection reactors for powers above 100 Kw.

N^{16}-gamma method is a counting method, that uses a gamma ionization chamber IC_γ. The output current is proportional to the N^{16}-gamma activity produced by high energy fission neutrons ($O^{16}(n,p)N^{16}$ reaction). If the effective coolant flow is constant the N^{16}-gamma activity is proportional to the total fission rate. It is very important to position the chamber far from the core to avoid fission and activation gammas detection, but not too much in order to avoid a large activity decay. It is necessary a calibration using another method to obtain the absolute power.

The statistical methods (one of them in the frequency domain is analyzed in this report) are nonperturbative and are based on the space independent point kinetic model. These methods need high absolute detectors efficiencies and also the predominance of fission density fluctuations as the correlated neutron noise source.

Under these assumptions the correlated part of the Power Spectral Density (PSD) is proportional to the total fission rate.

Absolute power determination using these techniques was first reported by Bennett (1960) who performed time-domain (variance) analysis in the ZPR-IV reactor at Argonne National Laboratory. Frequency domain analysis was proposed by Schroeder (1962). Subsequently, this noise technique has been performed by Yamada (1964), Suzuki et al (1966,1968), Mogilner and Shvetsov (1967), etc.

Statistical methods are affected by systematical errors because it is necessary to know the effective delayed fraction $\bar{\beta}$ and also to correct the spatial dependence of noise in case of using the point kinetic model.

Otsuka and Iijima (1965) were the first to propose a geometrical g-factor in order to correct the point kinetic model. This factor takes into account the non uniform spatial distribution of the static and adjoint fundamental mode fluxes. Saito (1979) derived a generalized expression using a multigroup diffusion fundamental mode model and made a review of several g-factor so far obtained. Okajima et al (1987) studied the trends of this factor for reflected reactor in one group approximation considering the reflector effect by a reflector saving. Wentzeis et al (1988) proposed a L_1 factor that takes into account the position and energy response of the detectors and the harmonics contribution in the detectors' field of view. Calculations were made using two-group diffusion model in multi-region geometries and a modal solution for the static and adjoint fluxes. The solution (for a small MTR swimming-pool type reactor) depends on detector position and the number of harmonics considered.

In this work the formulation developed by Difilippo (1990a and 1990b) was used to anlyze the contribution of the different modes in the PSD. The non correlated part of the neutron noise due to the detection process was explicitly considered. Systematical experimental determinations of the power were made in the MTR swimming pool graphite-water reflected RA-6 reactor.

For practical purposes the power estimation using this method should not be much sensible to different configurations such as reflector materials, detector locations, rod insertion, etc. This means from a theoretical point of view the predominance of the fundamental mode in detectors' fields of view in the formulation considered.

Experimental determinations and fitting of the PSD from two nearby core detectors changing the rod insertions were made in order to:

a) verify the predominance of the fundamental mode in the fitted region,

b) determine the power range of applicability (Predominance of fission density fluctuation as the correlated source of noise in the fitted region),

c) calibrate others neutron ionization chamber (IC) and an IC_{γ} sensible to N^{16}-gamma in order to measure higher power. This extension would allow a comparison with a calorimetric method.

II. FUNDAMENTALS OF THE METHOD

A. Theoretical Considerations

Applying the stochastic theory of nuclear reactions, it is possible to obtain a relation between the statistical fluctuation of the current from a IC and the stationary power of the critical reactor .

Following Difilippo (1990a and 1990b), the Fourier component of the neutron flux, Φ_ω, satisfies:

$$\hat{H}\,\phi_\omega + S_\omega = j\,\frac{\omega}{v}\,\phi_\omega(\vec{u}) \tag{1}$$

where $\hat{H}$ is the prompt neutron Boltzman operator, S_ω is the Fourier component of a generic source, "j" is the imaginary unit, "ω" is the angular frequency and "v" is the velocity of the neutrons, Φ_ω is a function of $\vec{u}$ where $\vec{u}$ is the position in phase space $\vec{r},\vec{v}$.

Our system is monitored with detectors (labeled i, ℓ) with cross sections $\Sigma_{di} = \Sigma_{di}(\vec{u})$, and so it is convenient to define the detector field of view η_i through the adjoint equation:

$$\hat{H}^{+}\eta_i + \Sigma_{di} = j\,\frac{\omega}{v}\,\eta_i \tag{2}$$

where $\hat{H}^{+}$ is the adjoint operator of $\hat{H}$. From Eqs. (1) and (2), the Fourier component of R_i, the detection reaction rate for detector i, can be obtained as:

$$R_{\omega i} = \langle \Sigma_{di}\,\phi_\omega \rangle = \langle \eta_i\, S_\omega \rangle \tag{3}$$

where the bracket indicates integration in phase space $\vec{u}$. The detector field of view can be expanded in terms of adjoint kinetic eigenfunctions:

$$\eta_i = \sum_{n=1}^{\infty} b_{in}\,\chi_n^{+}(\vec{u}) \tag{4}$$

where the χ_n^{+} satisfies:

$$\hat{H}^{+}\chi_n^{+} = -\frac{\alpha_n}{v}\,\chi_n^{+} \tag{5}$$

and α_n is the decay constant of mode n. We introduce now the direct kinetic eigenfunctions χ_m that satisfy:

$$\hat{H}\chi_m = \frac{\alpha_m}{V}\chi_m \tag{6}$$

with the normalization $\langle \chi_m \, 1/v \, \chi_n \rangle = \delta_{nm}$.

Introducing Eq. (4) into Eq. (2) and multiplying scalarly by χ_m we obtain:

$$b_{im} = \frac{\langle \Sigma_{di} \, \chi_m \rangle}{(\alpha_m + j\omega)} \tag{7}$$

where $\langle \Sigma_{di} \, \chi_m \rangle$ is a real, frequency independent quantity.

B. PSD Between Neutron Detectors

Applying the general result of Eq. (3), the contributions to the fluctuation of the signal from a source of noise around $\vec{u}$ are:

$$\delta R_{\omega i}(\vec{u}) = \eta_i \langle \delta S_\omega(\vec{u},\vec{u}') \rangle_{\vec{u}'} \tag{8}$$

and the cross power spectral density (CPSD) between detectors i and ℓ is:

$$G_{i\ell} = 2 \langle\langle \overline{\eta_i^*(\vec{u})\, \eta_\ell(\vec{u}')\, \delta S_\omega(\vec{u},\vec{u}')} \rangle\rangle \tag{9}$$

where the double brackets indicate integration in phase space $\vec{u}$ and $\vec{u}'$ and the upper line indicates ensemble average. Factor 2 appears because we are considering positive frequencies (Bendat and Piersol, 1981). Commuting operations in Eq. (9) and considering that the η's are deterministic, the ensemble average affects only the source of noise. The ensemble average of the source can be calculated applying the Schottky prescription (Akcasu and Stolle, 1989) and considering the angular correlation between fission neutrons (Difilippo, 1990b). Considering the detectors remove the detected neutrons and only type of fissionable material, the result is:

$$\overline{\delta S_\omega(\vec{u},\vec{u}')} = G_{ss}(\vec{u},\vec{u}') \tag{10}$$

where:

$$G_{ss}(\vec{u},\vec{u}') = 2\,\overline{\nu_p(\nu_p - 1)}\, f(\vec{r})\, \delta(\vec{r}' - \vec{r})\, \gamma_f(\vec{v}',\vec{v}) \tag{11}$$

is the auto power spectral density (APSD) of the statistical fluctuation of the fission density, $f(\vec{r})$ is the fission rate distribution, $\gamma_f(\vec{v}',\vec{v})$ is the two neutrons distribution in $\vec{v}',\vec{v}$. The index "p" refers to the prompt approximation, i.e. we assumed the frequency is well above (λ_i) the typical frequencies associated to delayed neutrons, thus the average over ν_p refers to the distribution of prompt fission neutrons in the fuel and might include average over fissionable species. After introducing Eq. (10) in Eq. (9), the CPSD is given by:

$$G_{i\ell} = \langle\langle \eta_i^* \eta_\ell \, G_{SS}(\vec{u},\vec{u}') \rangle\rangle \tag{12}$$

where $G_{SS}(\vec{u},\vec{u}')$ is given by Eq. (11).

Eq. (12) gives an incomplete description of the APSD ($i=\ell$) (Sheff and Albrecht, 1966). As the detector removes the detected neutron, the detection process destroys any single-neutron correlation which, otherwise, the neutron would have had in the future. Single-neutron effects contribute to the count-rate fluctuation; i.e. they appear only in the so called detection-noise component which is a (dominant) white noise term in the APSD. The detection noise process between two different detectors is uncorrelated. For this reason, the detection-noise is eliminated by a cross-correlation measuring device. Considering an ideal pulse mode detector (zero collection time in Appendix A) the PSD from Eq. (12) is:

$$^{(c)}G_{i\ell} = \langle\langle \eta_i^* \eta_\ell \, G_{SS}(\vec{u},\vec{u}') \rangle\rangle + 2\bar{R}_i \, \delta_{i\ell} \tag{13}$$

where: $\bar{R}_i = \langle \overline{\Sigma_{di} \phi} \rangle$: mean value of R_i

The first term in the right hand is known as "correlated-term" and the second as "uncorrelated-term".

In the case the neutron detector is a IC the current I is made up by many pulses of charge produced by the detection of individual neutrons. In this case the uncorrelated-term in Eq. (13) increases due to the statistics of the detection in the IC and includes the charge $q_{n,i}$ released per detected neutron. Considering an ideal IC (see Appendix A) Eq. (12) is:

$$\frac{^{(I)}G_{i\ell}}{\bar{q}_i \bar{q}_\ell} = \langle\langle \eta_i^* \eta_\ell \, G_{SS}(\vec{u},\vec{u}') \rangle\rangle + 2 B_i \bar{R}_i \, \delta_{i\ell} \tag{14}$$

where $\mathbb{B}_i = \overline{q_i^2}/(\overline{q_i})^2$ is the Bennett factor (>1) (Bennett , 1960).

A realistic IC has a finite pulse collection time $\tau_i = 2\pi / \omega_{ci}$ (ω_{ci}: angular break frequency of the detection device) and the measurement may be strongly influenced by the statistics of the detection process at frequencies near "ω_{ci}". In this case Eq. (14) is written:

$$\frac{{}^{(I)}G_{il}}{\bar{q}_i \bar{q}_l} = \left[\langle\langle \eta_i^* \eta_l \, G_{ss}(\vec{u}, \vec{u}') \rangle\rangle + 2\mathbb{B}_i \bar{R}_i \, \delta_{il} \right] h_i^* h_l \tag{15}$$

where $h_i(\omega)$ is the transfer function of the IC_i (see Appendix A).

C. Estimation of the Power

The PSD's can be calculated by an adecuate approximation of the Boltzman operator $\hat{A}$, using a multigroup model, S_n or P_n angular expansions, spatial dependent models. $\xi(\vec{u})$ and η_i's can be evaluated using a closed solution or a modal type expansion solution. Only in a few cases a closed solution can be derived.

In our case a modal expansion of the detectors' field of view was used and the CPSD for ideal pulsed detection devices (Eq. (12)) can be written as:

$$G_{il} = \sum_{n=1}^{\infty} \frac{A_{il}^{(n)}}{\left(1 + \frac{\omega^2}{\alpha_n^2}\right)} + j\omega \sum_{i=1}^{\infty} \frac{B_{il}^{(n)}}{\left(1 + \frac{\omega^2}{\alpha_n^2}\right)} \tag{16}$$

where:

$$A_{il}^{(n)} = \frac{1}{\alpha_n} \sum_m F_{nm} \, C_{il}^{(n,m)} \tag{17}$$

$$B_{il}^{(n)} = \frac{1}{\alpha_n^2} \sum_m F_{nm} \, D_{il}^{(n,m)} \tag{18}$$

$$F_{nm} = \frac{\langle\langle \chi_n^+(\vec{u}) \, \chi_m^+(\vec{u}') \, G_{ss}(\vec{u}, \vec{u}') \rangle\rangle}{(\alpha_n + \alpha_m)} \tag{19}$$

$$C_{il}^{(n,m)} = \langle \Sigma_{di} \chi_n \rangle \langle \Sigma_{dl} \chi_m \rangle + \langle \Sigma_{di} \chi_m \rangle \langle \Sigma_{dl} \chi_n \rangle \tag{20}$$

$$D_{il}^{(n,m)} = \langle \Sigma_{di} \chi_n \rangle \langle \Sigma_{dl} \chi_m \rangle - \langle \Sigma_{di} \chi_m \rangle \langle \Sigma_{dl} \chi_n \rangle \tag{21}$$

If the condition $|\alpha_k| >> |\alpha_1|$ k=2,3,... is fulfilled,in the frecuency region $\omega << \alpha_K$ the main contribution in Eq.(16) is :

$$G_{i\ell}^{(1)} = \frac{A_{i\ell}^{(1)}}{\left(1+\frac{\omega^2}{\alpha_1^2}\right)} + j\omega \frac{B_{i\ell}^{(1)}}{\left(1+\frac{\omega^2}{\alpha_1^2}\right)} \tag{22}$$

Eq. (17) to (21) show that the amplitudes $A_{i\ell}^{(1)}$ and $B_{i\ell}^{(1)}$ depend on higher harmonics contamination.

Assuming that the contribution to the detectors field of view in Eq.(4) is mainly due to the first term ($b_{in}=0$ for n>1):

$$G_{i\ell}\Big]_{fm} = \frac{\langle \Sigma_{di}\chi_1\rangle \langle \Sigma_{d\ell}\chi_1\rangle \langle\langle \chi_1^+(\vec{u})\chi_1^+(\vec{u}')\, G_{SS}(\vec{u},\vec{u}')\rangle\rangle}{\left(1+\frac{\omega^2}{\alpha_1^2}\right) \qquad \alpha_1^2} \tag{23}$$

This means that the detectors field of view are distributed according to the fundamental adjoint kinetic eigenfunction . This is the only case where the higher harmonics don't contributes to the $G_{i\ell}$.

Assuming small anisotropy (f.e : diffusion theory validity), the Eq. (23) can be written as :

$$G_{i\ell}\Big]_{fm} = \frac{A_{i\ell}\Big]_{fm}}{\left(1+\frac{\omega^2}{\alpha_1^2}\right)} = G_{i\ell}\Big]_{PK}\, g_{i\ell} \tag{24}$$

where :

$$G_{i\ell}\Big]_{PK} = \frac{2\,\bar{F}\,\varepsilon_i\,\varepsilon_\ell\,(1-\bar{\beta})\,D}{\left(1+\frac{\omega^2}{\alpha_1^2}\right)\bar{\beta}^2} \tag{25}$$

The factor $g_{i\ell}$ must be obtained from calculation, according to :

$$g_{i\ell} = \left[\frac{\int_{\vec{r}} f(\vec{r})\left(\int_E \chi_1^+(\vec{r},E')\,S(E')\,dE'\right)^2 d^3r}{\bar{F}}\right]\frac{(\Lambda\bar{\nu})^2\langle\Sigma_{di}\chi_1\rangle\langle\Sigma_{d\ell}\chi_1\rangle}{\varepsilon_i\,\varepsilon_\ell} \tag{26}$$

S(E') : fission spectrum

$\bar{F} = \int_{\vec{r}} f(\vec{r})\,d^3r$:mean total fission rate (27)

$\varepsilon_i = \frac{\bar{R}_i}{\bar{F}}$:absolute detector efficiency (28)

$\bar{\beta}$: delated effective neutron fraction = $\Lambda\alpha_1$ (29)

$$\Lambda = \frac{\langle \phi / v \rangle}{\bar{F}\,\bar{\nu}} \quad : \text{ reproduction time} \tag{30}$$

$$\overline{\nu(\nu-1)(1-\bar{\beta})} = \overline{\nu_p(\nu_p-1)} \tag{31}$$

$$D = \frac{\overline{\nu(\nu-1)}}{\bar{\nu}^2} \quad : \quad \textit{Diven Factor} \tag{32}$$

In the case of one-group infinite-homogeneous critical reactor with an infinite-homogeneous detector, $g_{i\ell} = 1$ and $G_{i\ell}]_{fm}$ reduces to the expression obtained by the point kinetic model. For that reason, $g_{i\ell}$ could be considered as a correction factor to the point-kinetic model. This factor is different of the g-factor used by Otzuka because takes into account explicitly the detectors.

From Eqs. (24) and (25) is possible to obtain the stationary reactor power from the estimator $P_{i\ell}]_{fm}$ defined as:

$$P_{i\ell}]_{fm} = \bar{E}_f\,\bar{F} = \frac{2\,\bar{E}_f\,\bar{R}_i\,\bar{R}_\ell\,(1-\bar{\beta})\,D\,g_{i\ell}}{A_{i\ell}]_{fm}\,\bar{\beta}^2} \tag{33}$$

where: $\bar{E}_f$ is the mean energy released by fission, $\bar{R}_i$ and $\bar{R}_\ell$ are obtained from the count rates and $A_{i\ell}]_{fm}$ can be obtained from the experimental PSD, in an ideal situation, where the detectors' field of view are distributed according to the fundamental adjoint kinetic eigenfunction.

In a real case, the fundamental mode approximation, is not strictly valid and the harmonic contamination could be important according with the reactor characteristic.

In the case of a critical compact reactor, the prompt neutrons decay constants are well separated (see Appendix B). For this reason it could be possible to find a frequency region where the first term (real)in Eq. (16) is predominant.

Measurements made by Lescano and Behringer (1982), in the SAPHIR swimming-pool partially water-berylium reflected MTR reactor and Piñeyro et al (1983) in the RA-2 MTR critical facility in different partially reflected (graphite or beryllium) configurations founded that $G_{i\ell} \cong Re(G_{i\ell}^{(1)})$ (Re : real part) between 1 and 40 Hz (partial reflected Beryllium), 1 and 80 Hz (partially reflected graphite) and 1 and 100 Hz (totally water reflected).

In this case, can be defined a factor L_1 that takes into account the harmonic contamination in $A_{i\ell}^{(1)}$ (see Eq. (17)) and considering a non ideal detector, particularly a IC, the expression for normalized PSD (NPSD) in these frequency regions is:

$$\frac{{}^{(I)}G_{i\ell}}{\bar{I}_i \bar{I}_\ell} \simeq \frac{Re\left({}^{(I)}G_{i\ell}^{(1)}\right)}{\bar{I}_i \bar{I}_\ell} = \frac{2\bar{F}\mathcal{E}_i\mathcal{E}_\ell(1-\bar{\beta})D\,\bar{q}_i\bar{q}_\ell L_1}{\bar{\beta}^2\,\bar{I}_i\bar{I}_\ell\left(1+\frac{\omega^2}{\alpha_1^2}\right)} + \frac{2\bar{F}\mathcal{E}_i\overline{q_i^2}}{\bar{I}_i^2}\,\delta_{i\ell} \qquad (34)$$

where:

$$\bar{I}_i = \mathcal{E}_i \bar{F}\,\bar{q}_i : \text{ mean current of i-th IC} \qquad (35)$$

Having all these considerations in mind, the stationary reactor power can be obtained from the estimator $P_{i\ell}^{(1)}$ defined as:

$$P_{i\ell}^{(1)} = \frac{2\,\bar{E}_f\,D\,(1-\bar{\beta})\,L_1}{{}^{N}A_{i\ell}^{(1)}\,\bar{\beta}^2} \qquad (36)$$

${}^{N}A_{i\ell}^{(1)}$ is experimentally obtained from:

$${}^{N}A_{i\ell}^{(1)} = \frac{{}^{(I)}G_{i\ell}(\omega \ll \alpha_1) - {}^{(I)}G_{DD}\,\delta_{i\ell}}{\bar{I}_i\,\bar{I}_\ell} \qquad (37)$$

where:

$${}^{(I)}G_{DD} = {}^{(I)}G_{ii}\left(\alpha_1 \ll \omega \ll \omega_{ci}\right) \qquad (38)$$

D. Considerations about the application of the method.

Eq. (36) is the basis of the proposed method to measure the stationary reactor power using ICs.

The $\bar{E}_f$=3.2x10^{-11}J (ISO, 1988) and D=0.795 (Diven et al, 1956) parameters for high U-235 enriched fuel elements were chosen. The $\bar{\beta}$ and L_1 parameters were calculated numerically . The $^{N}A^{(1)}_{i\ell}$ was obtained fitting the experimental normalized PSD (NPSD) ($^{(I)}G_{i\ell}/\bar{I}_i\bar{I}_\ell$) in a frequency region where $^{(I)}G_{i\ell}$ =Re($^{(I)}G^{(1)}_{i\ell}$).

The value of $\bar{\beta}$ and L_1 depend principally on: geometry of the configuration, reflector type, control rods insertion, fuel burn-up and additionaly for L_1: locations, dimensions and energy response of detectors.

Uncertainty in nuclear parameters or approximation used in the calculations would produce a systematic error in the proposed method. It is possible to obtain an estimation of this error studying the variation of $\bar{\beta}$ and L_1 respect to the nuclear parameters during a reactor cycle.

Wentzeis et al (1988) calculated L_1 and a value equal to 1.19 was obtained for the MTR graphite-water reactor considered. Also it was analyzed the influence of nuclear parameters on L_1, using a 3D two group diffusion model and a modal solution for the detector field of view. Strong changes of typical nuclear parameters (~20%) affect in less than 1.5 % the L_1 value.

Higa M.(1990) calculated $\bar{\beta}$ = 0.0078 for the reactor considered, the variation of $\bar{\beta}$ with respect to nuclear parameters also was analyzed and it was founded that strong variations (~20%) affect less than 1% the $\bar{\beta}$ calculated.

In order to obtain A (A = $^{N}A^{(1)}_{i\ell}$) by fitting the experimental values it is necessary to have high absolute detectors efficiency because of the following considerations:

The function proposed to fit the NPSD is (in dB):

$$F(\omega)= 10 \log\left[\frac{A}{(1+\frac{\omega^2}{\alpha^2})} + N\,\delta_{i\ell}\right] \qquad (39)$$

where :

$$N= \frac{^{(I)}G_{DD}}{\bar{I}_i^{\,2}} \qquad (40)$$

A, α and N are the fit parameters.

For the APSD case it is reasonable to propose the following:

$$A > N \tag{41}$$

The detector efficiency obtained from Eq. (34) is:

$$\varepsilon_i = \frac{\bar{\beta}^2 \mathbb{B}_i A}{L_1 D(1-\bar{\beta}) N} \tag{42}$$

A minimum absolute detector efficiency, ϵ_{mi} can be defined considering the inequality (41):

$$\varepsilon_i > \varepsilon_{mi} = \frac{\bar{\beta}^2 \mathbb{B}_i}{L_1 D(1-\bar{\beta})} \tag{43}$$

For a typical high enriched compact reactor ($\bar{\beta}$=7.8x10^{-3}, L_1=1.19, D=0.795) and considering IC with $\mathbb{B}_1 \cong 1$ a $\epsilon_m \cong (\bar{\beta})^2$=6.5x$10^{-5}$ was calculated from Eq. (43). Otherwise, in order to avoid a high perturbation in the nuclear system , it is necessary that $\langle \overline{\Sigma_{d1} \Phi} \rangle \ll \bar{F}$. This means there is a practical ϵ maximum, $\epsilon_M \cong 10^{-3}$ in Eq. (28).

For the CPSD case, the experimental data have a dispertion $\sigma_{1\ell}$ given by (Bendat and Piersol, 1981):

$$\frac{\sigma_{i\ell}(\omega)}{|{}^{(I)}G_{i\ell}(\omega)|} = \frac{1}{\sqrt{\Delta f \, T_M \, \gamma_{i\ell}^2}} \tag{44}$$

where:

Δf: resolution bandwidth = BW/n_p ,

T_M: measurement time,

BW: bandwidth,

n_p: number of points in BW.

$$\gamma_{1\ell}(\omega) = \frac{{}^{(I)}G_{1\ell}}{\sqrt{{}^{(I)}G_{11} \, {}^{(I)}G_{\ell\ell}}} \quad \text{coherence function} \tag{45}$$

Considering $\Psi = 10\log(|^{(I)}G_{i\ell}|)$, results:

$$\sigma_\Psi \cong \frac{4}{\sqrt{\gamma_{i\ell}^2\left(\frac{BW}{n_p}\right)T_M}} \quad \text{(in dB)} \tag{46}$$

Introducing Eq. (34) into (45) we obtain:

$$\gamma_{i\ell}^2(\omega) = \frac{\varepsilon_i\varepsilon_\ell}{\varepsilon_i\varepsilon_\ell + \left(1+\frac{\omega^2}{\alpha_1^2}\right)(\varepsilon_{mi}\varepsilon_\ell + \varepsilon_{m\ell}\varepsilon_i) + \left(1+\frac{\omega^2}{\alpha_1^2}\right)^2\varepsilon_{mi}\varepsilon_{m\ell}} \tag{47}$$

Eq. (47) shows that $\gamma_{i\ell}^2$ increases with ϵ_i and ϵ_ℓ and decreases with ω. A "minimum coherence", "γ_m" is obtained considering $\epsilon_i=\epsilon_\ell=\epsilon_{mi}=\epsilon_{m\ell}$:

$$\gamma_m^2(\omega) = \frac{1}{1+2\left(1+\frac{\omega^2}{\alpha_1^2}\right)+\left(1+\frac{\omega^2}{\alpha_1^2}\right)^2} \tag{48}$$

Considering $0<\omega<\alpha_1$ as the fitted region, we obtained $\gamma_m^2(0)=1/4$ and $\gamma_m^2(\alpha_1)=1/9$. Introducing $\gamma_m^2(\alpha_1)$ in Eq. (46):

$$\sigma_M \cong 12 \times \sqrt{\frac{n_p}{BW \times T_M}} \quad \text{(in dB)} \tag{49}$$

σ_M is the maximum CPSD data deviation when the minimum efficiency ε_m is considered.

A criteria to select T_M in Eq. (49) is propose that $2\sigma_M < 3$ because the CPSD at $\omega=\alpha$ is aproximately 3dB lower than the CPSD at $\omega\cong 0$. If $n_p=256$ the measured time is $T_M > (273/BW)$ min.

The main hypothesis to verify in the fitted frequency region are:

<u>hypothesis 1: the fission rate fluctuation is the predominant noise source.</u>

Robinson (1967) showed that in power reactors other noise sources have to be considered such as thermohidraulic process, internal components vibrations, etc. These sources produce fluctuation in the reactivity. If this fluctuation is independent of the fission rate fluctuation , the source term in Eq. (11) must be written:

$$G_{ss}(\vec{r},\vec{r}\,') + P^2 G_{\rho\rho}(\vec{r},\omega) \longrightarrow G_{ss}(\vec{r},\vec{r}\,') \tag{50}$$

where:

$G_{\rho\rho}(\vec{r},\vec{r}')$: APSD of the reactivity fluctuation.

The two terms in Eq. (50) depend in a different way on the reactor power so it is possible to distinguish them experimentally. In case that in the fitted region the inequality $P^2G_{\rho\rho} \ll G_{SS}$ were not valid, the power estimation using the proposed method would not have a lineal dependence respect to other methods. These methods could be : the absolute counting method using a IC, N^{16}-gamma detection, foil activation, calorimetric method, etc.

hypothesis 2: the fundamental mode is the predominant one.

If this were not valid for a given power, the values of the fitted parameters A, α, should change more than the experimental error for different control-rods configuration, detectors locations etc. This is a experimental way to verify this hypothesis.

E. Power Limits of the method:

The considerations analyzed in section **D** implie a maximum limit for the power. The following conditions must be fulfilled:

a) $P^2G_{\rho\rho} \ll G_{SS}$, in Eq. (50), (51)

b) $\bar{I}_i < I_S$, (52)

where $\bar{I}_i$ is the mean current and I_S is the saturation current of the i-th IC.

As power increases, the term $P^2G_{\rho\rho}$ increases respect to G_{SS}, specially at low frequencies. To avoid this contribution, it is necessary to begin the PSD fitting at higher frequencies. This reduces the amount of spectra points and also these points have higher standard deviation due to the lower coherence. These two effects increase the error in the power estimation.

Also a minimum limit for the measured power has to be considered. It is necessary that:

a) ${}^{(v)}G_{ii}{}^{(BK)} \ll {}^{(v)}G_{ii}$ (53)

where:

${}^{(V)}G_{ii}$: APSD for the critical stationary reactor at the detection device output (see Figure 2).

${}^{(V)}G_{ii}^{(BK)}$: background electric noise APSD from the detection device.

b) $I_{fi} \ll \overline{I}_i$ (54)

where :

I_{fi}: leakeage current of the i-th IC.

c) reasonable stability of reactor at low powers

Both ${}^{(V)}G_{ii}^{(BK)}$ and I_{fi} are not originated in the reactor, so they are not proportional to the reactor power.

III. EXPERIMENTAL PART

A. Description of the Detection, Acquisition and Analysis Data System

Measurements were made in the RA-6 reactor. An scheme of the reactor configuration and detectors' locations is shown in Figure 1. Three neutron compensated IC labeled IC_1, IC_2, IC_3 and one gamma IC_γ were used

Figure 2 shows an scheme of the detection, acquisition and analysis data system. The noise amplifier Am_i convert the current I_i in proportional voltages V_i. The mean values $\overline{V_i}$ were measured using a digital voltmeter and the fluctuations δV_i were amplified by a factor K_i=100. The current $\overline{I_N}$ from the IC_γ was measured using an electrometer.

The fluctuations ($K_i \cdot V_i$) were digitalized and frequency analyzed by a HP-5420A signal analyzer interfased to a PC in order to obtain the normalized PSD, ψ_N (in dB) :

$$\psi_N = 10 \log \left[\frac{|G_{il}^{(v)}|}{(K_i K_l \overline{V_i}\,\overline{V_l})} \right] = 10 \log |NPSD| \qquad (55)$$

These values were fitted using the Marquardt's method and the function $F(\omega)$ defined in Eq. (39). In the BW 0-200 Hz the fitted parameters were A, N, and α and in the BW 0-25 Hz A, α and the N fitted before was used. ϵ_i, was obtained from Eq. (42) and the estimators P_{il} and $f_i^{(q)}$ defined in Eqs. (36) and (A-6), were obtained from:

$$P_{il} = \frac{2\overline{E_f}\, D(1-\overline{\beta}) L_1}{A\, \overline{\beta}^2} \qquad (56)$$

$$f_i^{(q)} = \frac{N}{2}\, \overline{I_i} \qquad (57)$$

B. Previous Measurements

In order to check the conditions discussed in section II.E, analyze the $f_i^{(q)}$ given by Eq.(57) and measure the transfer function h_i previous measurements were made.

The detectors IC_1 and IC_2 were located at positions p_1 and p_2 (Fig.1) far from the core and at positions I7 and H1 (the nearest the core) at different current values.

The currents I_{fi} and the background electric noise PSD $^{(v)}G^{(BK)}$ were measured being the reactor shutdown and the values obtained were:

i) $I_{fi} < 10^{-2}\bar{I}_i$, $\quad {}^{(v)}G_{ii}^{(BK)} < 10^{-3} \cdot {}^{(v)}G_{ii}$ for $\bar{I}_i > 10^{-9}$ A,

So the conditions required in Eqs. (53) and (54) were fulfilled.

ii) $^{(v)}G_{ii}$, the transfer function h_i and $f_i^{(q)}$ were obtained with detectors located at p_1 and p_2, ϵ_i and again $f_i^{(q)}$ were obtained with detectors located at I_7 **and** H_1. The ϵ_i measured was $\epsilon_i \cong 1\times10^{-4}$. The condition required in Eq.(43) was fulfilled. Using this value and Eq. (35) , the ϵ_i for detectors located at p_1 and p_2 was calculated: $\epsilon_i \cong 10^{-8} \ll (\bar{\beta})^2$.

It means the detection term is the predominant one in Eq. (43) for detectors located far from the core,

iii) the Transfer Function is flat between 1 and 300 Hz. It shows a low frequency cut off at about 0.2 Hz due to the filter used to cut the continuous component of the signal and a high frequency cut off (f_{ci}) at about 1.5 KHz,

iv) the $f_i^{(q)}$ values obtained (see Figure 3) don't depends on the detectors' efficiency. It means that near the core the fitted function considered was the adequate in order to discriminate the uncorrelated from the correlated term. This parameter depends on the detection process statistics only as it is explained in the Appendix A. In our measurements $f_i^{(q)}$ were used as a criteria to estimate the correct detection device operation. The values having an error greater than three times the standard deviation (σ) were rejected. Figure 3 also shows the $f_i^{(q)}$ value obtained with IC's voltage outside the plateau region in order to apply the rejection criteria. In this case the detection noise variation was much more sensitive than the mean current variation,

v) the chamber IC_3 was positioned in p_3 (Figure 1) in order to use it within all the reactor power range. IC_γ was located in p_4 far from the core in order to avoid fission or activated gammas.

C. Measurements at Different Powers

Measurements were made at 9 steps from 10 W to 5 Kw to obtain the thermal power from Eq.(56) and to verify experimentally the hyphotesis 1 and 2 explained in section II.D (series 1 to 3 in Table I).

The results were used to calibrate the IC_3 and the IC_γ in order to measure higher powers (series 4 and 5 in Table I).

Two different rod insertions were considered for control rods B3 and B4 (Fig. 1) in order to perturb the flux measured by IC_1 and IC_2 and a study of this perturbations on the proposed method was made. The maximum reactivity excess accepted by the Regulatory Authority forbids more control rod insertion. Nevertheless the perturbation was important because the reactivity value of the control rods are B3: (3.61 ± 0.15)$ and B4: (4.10 ± 0.06)$ (Waldman and Gomez, 1988 - Gomez and Waldman, 1989).

From Table I two different control rods configurations can be defined:

Configuration I (B1=B2=B4=100%↑, B3=45%↑)

Configuration II (B1=B2=B3=100%↑, B4=50%↑)

In each power step ~10 min were awaited to ensure reactor stability and different series of three values of $P_{i\ell}$ using Eq. (56) were obtained, two using a BW = 0-25 Hz, T_M = 15 min and one using BW = 0-200 Hz, T_M = 15 min. With these values, the condition required for σ_M<3 dB (Eq. 49) were fulfilled.

From this $P_{i\ell}$'s values the mean weighted value $\overline{P_{i\ell}}$ was calculated.

In each of the previous series power changes should implies a proportional current change from the ICs. In order to verify this behaviour I_2 was selected as a reference and the other currents were fitted respect to I_2. Figure 4, for example, shows the results for serie 1.

Hyphotesis 1 and 2 considered in section II.D were verified through a lineal regression between the differents $P_{i\ell}$ and I_2, and the values of the fitted parameters are shown in Table II. The goodeness of the linear behaviour for each serie implies the validity of hyphotesis 1. It is seen that the coefficient $a_{i\ell}^{(S)}$ (inverse of the fitted parameter A) for different detectors are similar in each of the series. They agree aproximately between 2σ and this means hyphotesis 2 is valid. Similar values of α (between σ) for the different series is also a verification of hyphotesis 2. The values were obtained from the CPSD in the BW = 0-25 Hz. The extrapolated $b_{i\ell}^{(S)}$ values show that this calibration is valid for powers higher than 100 w (σ=1%).

These considerations allow us a better estimation of the power P as the weighted mean values of $\overline{P_{11}}$, $\overline{P_{22}}$ and $\overline{P_{12}}$ at each serie and power step. There is a lineal relation between P and I_i (i=1, 2, 3) as shown in Table III and in Figure 5 for I_3.

Considering Table III we can comment the following:

a) there is no difference in the calibration factor $m_1^{(S)}$ using natural or forced convection,

b) different control-rods insertions affect in a different way the calibration of the IC's current. The calibration $m_1^{(S)}$ factor change -3% for IC_1, +10% for IC_2 and -13% for IC_3,

c) $\overline{I_3}$ calibration was used to calibrate $\overline{I_N}$ in forced convection and higher powers. This calibration was independent of control rods positions (between σ). The calibration factor for $\overline{I_N}$ was $(2.803 \pm 0.042)\times10^{14}$ W/A (valid for $\overline{I_N} > 10^{-10}$ A).

Another calibration made by calorimetric method gave $(2.59\pm0.30)\times10^{14}$W/A (Blaumann et al (1987)) i.e. similar value but with a standard deviation value 7 times higher.

Figures 6 to 10 shows the noise functions obtained during the same measurement of serie 1 at 5 Kw with their fitted parameters.

Figures 6 and 7 are NAPSD with BW= 0-200 Hz and BW= 0-25 Hz respectively. The value of N obtained from Fig.6 was used to fit the NAPSD in Fig.7 to reduce the error in the power estimation. The values of ϵ_1 obtained were higher than $(\overline{\beta})^2$.

Figures 8 and 9 are NCPSD measured with BW= 0-200 Hz and 0-25 Hz respectively. Values of the power and α with lower errors were obtained from the second case. This errors were aproximately 3-4%. Figure 8 shows an increase in the NCPSD values dispertion at frequencies higher than 50 Hz. This can be explained considering the low coherence due to the predominant contribution of the detection noise in this frequency region. Using Eq. (46) for f=100 Hz, σ_ψ is about 5.2 dB. This value is higher than the 3 dB suggested in section II.D. This high dispertion makes very difficult the experimental verification of higher modes contributions within this frequency region. A shift between the experimental data and the extrapolated function considered is observed.

Figure 10 shows a typical coherence and is clearly seen that it is higher than the γ_m value defined in Eq. (48) for $0 < \omega < \alpha$. Introducing $\gamma_{12}(\omega=\alpha) = 0.18$ in Eq. (46) results $\sigma_\psi = 0.8 \times \sigma_M \cong 1$ dB. The experimental data of the NCPSD have a typical deviation of the curve regression of 0.86 dB.

Figure 11 shows a NCPSD for a serie 2 measurement also at ~5 Kw. There is an increment of the NPSD at low frequencies respect to the NCPSD in Fig. 9. This is due to the appearance of another noise source due to forced convection. In this case in order to be valid hyphotesis 1, it is necessary to start the fitting process at higher frequencies. This produces a higher error as was explained in Section II.E.

Figure 12 shows a NCPSD at ~56 Kw corresponding to a measurement in serie 5. It was necessary to go to higher frequencies than the case showed before in Fig. 11. The value of the power obtained from the NCPSD was P = (56 $\pm$ 5) Kw similar to that from the $\bar{I}_N$ measurement P = (55.2 $\pm$ 1.6) Kw . The error of the P from the NCPSD is higher than the error from the $\bar{I}_N$ measurement.

Figure 13 shows the NCPSDs at ~5 Kw and~56 Kw. The different shape of the spectra in the low frequency region was explained in Section II.D considering the contributions due to mechanical components vibrations (peaks) and feedback thermohydraulics process (continuous). Both contributions increase in a different way with power.

Figures 14 and 15 show the NCPSD for natural convection at about 50 Kw using a BW=0-200 Hz and 0-25 Hz respectively. The control rods configuration and the $\bar{I}_N$ value was similar to the measurement showed in Figure 12.

Figure 14 shows an increase in the NCPSD in the low frecuency region (<20 Hz). At this power value (in natural convection) the feedback effect at the noise source due to the increase of the coolant temperature is important . In order to verify hypotesis 1 again it is neccesary to fit the NCPSD at higher frecuencies. The value of the power obtained was similar to the measurement made using forced convection, but the error was higher due to the low coherence in this fitted region. Figure 15 shows that the fitted parameters in the low frecuency region gave a wrong value of the power due to the higher contribution of the noise from inlet temperature fluctuations.

IV. CONCLUSIONS:

A minimum efficiency criteria was obtained by considering the influence of the detection noise in the dispertion of spectral data . The minimum efficiency must be $\epsilon_m > (\bar{\beta})^2$.

The $f_i^{(q)}$ parameter that depends on the statistics of the detection process was used as a criteria to estimate the correct operation of the detection device. The measurements showed that the estimation of that parameter was independent of the detector's efficiency.

Measurements were made in the RA-6 reactor, varying the insertion of two control-rods in natural and forced convection. It was verified experimentally the validity of the predominance of the fission density noise and the fundamental mode in the fitted spectral regions.

The method was applied to measure power in the 10 W to 5 Kw range and a standard deviation lower than 3% was obtained using one or two IC. The lower power limit depens on reactor stability and absolute detector efficiency. The upper limit depends on the IC lineal work range, absolute detector efficiency and feedback effect and vibration of internal components.

The method was applied to calibrate a third IC_3 sensitive to neutrons and one IC_γ sensitive to N^{16}-gamma. This calibration allowed us to measure until 200 Kw with a standard deviation lower than 2%. For powers higher than 5 Kw the value obtained from this calibration is similar to the noise measurement in forced convection but it has a lower error. The calibration of $\overline{I_N}$ was similar than the calibration by a calorimetric method but with 7 times lower statistic error.

ACKNOWLEDGEMENTS:

The authors are grateful to the following coleagues from CNEA: personal of RA-6 Reactor Division for operating the reactor, A. Pereyra for his help in the instalation of equipments for the measurements and Dr V. Lescano for his commentaries. We should also like to acknowledge the suggestions and reading of the manuscript by Dr F. Difilippo from ORNL (USA).

REFERENCES:

- Akcasu A. Z. and Stolle A. (1989). Comments on the noise Equivalent Source in the Langevin Technique, Ann. Nucl. Energy 16, 10.

- Bendat J. S. and Piersol A. G. (1981). Engineering Applications of Corretation and Spectral Analysis, John Wiley & Sons, New York.

- Bennett F. (1960). The rice forumulation of pile noise, Nucl. Sci. Engng. 8,53.

- Blaumann H., Larrieu Calzetta O., Gennuso G. (1987). Medición de Potencia del Reactor RA-6 por N^{16}, AATN, Reunión Científica, Bariloche 26-30 de Octubre.

- Difilippo F. C., (1987). Changes on the Statistics of Signals Because of the Action of Measuring Devices. Private Comunication.

- Difilippo F. C. (1990a). Harmonic Analysis of stochastic Descriptors and the Interpretation of ^{252}Cf Neutron Source Experiments. Accepted May 25, 1989, Nucl. Sci. and Engng.

-Difilippo F. C., (1990b). The Correlation Between Fission Neutrons and the Calculation of Stochastics Descriptors. Application to the ^{252}Cf Method, submitted to Nucl. Sci. and Engng.

- Diven B.C., Martin H.C, Taschek R.F. and Terrell J (1956) - Multiplicities of Fission Neutrons, Phys.Rev.,101:1012.

- Gomez A., Waldman R. (1989). Aplicacion de un método de "rod-drop" basado en la Teoría de Transporte para medir la efectividad de barras de control, CNEA-GI-1198/89.

- Higa M. (1990). Fraccion efectiva de neutones retardados del reactor RA-6, CNEA-Re-CA90-17.

-ISO/TC 85/SC 3/WG 11 N 51 (1988). Calculation of the decay heat power in nuclear fuels of light water reactors.

- Lescano V. H. and Behringer K. (1982). Investigation of Space-Energy Effects in the Reactivity Measurements by Neutron Noise Analysis with ex-core Detectors in a Reflected LWR, Ann. Nucl. Energy 9, 443.

- Mogilner A. I. and Shvetsov D. M. (1967). Statistical methods of measuring the absolute power of a reactor, J. nucl. Energy 21, 87.

- Okajima S., Narita M. and Kobayashi K. (1987). Simple Determination of Low Power on Reflected Reactors using the Feynman- Experiment., Ann. Nucl. Energy 14, 12, 673.

- Otsuka M. and Iijima T. (1965). Space-dependent formula for Rossi- measurements, Nukleonik 7, 488.

- Piñeyro J., Waldman R., Lescano V. (1983). Mediciones de las Funciones de Ruido en el Reactor RA-2. CNEA-GI-1034/83.

- Robinson J. C. (1967). Analysis of Neutron Fluctuation Spectra in the Oak Ridge Research Reactor and the High Fluc Isotope Reactor, ORNL-4149.

- Saito K. (1979). Source Papers in Reactor Noise, Progress in Nuclear Energy, 3, 157.

- Schroder R. (1962). Bestimmung der Reaktorleistung mit Hilfe des Reaktorrauschens, Nukleonik 4, 227.

- Sheff J. R. and Albrecht R. W. (1966). The space dependence of reactor noise I- Theory, Nucl. Sci. Engng. 24, 246, II- Calculation, Nucl. Sci. Engng. 26, 217.

- Suzuki E. (1966). A method for measuring absolute reactor power through neutron fluctuations, J. nucl. Sci Technol. 3, 98.

- Suzuki E., Nomura T. and Tsunoda T. (1968). Application of noise analysis to powr reactor control, preprints of Japan-Us Seminar on Nuclear Reactor Noise Analysis,pp. 87-101.

- Waldman R., Gomez A. (1988). Utilizacion de un sistema de adquisicion de datos para medir la efectividad de barras de control, empleando el modelo de la Cinetica Puntual ("Reactimetro digital"), CNEA-GI-1197/88.

- Wentzeis L., Gomez A., Laggiard E., Waldman R. (1988). Estudio Analítico del factor de forma que interviene en la estimación de la potencia térmica de un reactor nuclear usando la técnica de ruido neutrónico, CNEA-GI-1196-88.

APPENDIX A: Detection Process.

Figure A-1 shows the influence of the detection device on the APSD (for simplicity, the subindex characterizing the detector is not written).

The mean detection reaction rate, $\overline{R_i}$, depends on the total fission rate F and the absolute efficiency of the detector, ϵ_i. The fluctuation depends on the statistics of the neutron process viewed by the detector.

Two types of detection devices are used in noise analysis: pulsed mode and current mode. Pulsed mode detectors are usually used in measurements with low $\overline{R_i}$, i.e., in stationary subcritical states to obtain the fundamental prompt constant, to investigate the contribution of armonics (spatial-effects), and to estimate low-state power in a critical state. In power estimation, counting rate values C_i have to be optimized to avoid dead time corrections when $\overline{R_i}$ are very high. On the other hand, high absolute detection efficiencies are necessary, then detectors should be located near or inside the core. In case of higher power it is necessary to use IC near the core.

In a typical neutron detector, the detection of one neutron, produces one or more heavy charged particles that ionizates the detector gas molecules (including multiplication process) producing a charge $q_{n,i}$. The charged particles are electrons with a collection time t_i^- and ions with a collection time t_i^+. The charge $q_{n,i}$ is too low for practical purposes.

In the pulsed mode, the pulse charge related to q_{ni} is conformed and amplified in order to produce a narrow and tall voltage pulse. This pulse has a time duration $\sigma_{pi} \sim t_i^-$. As all pulses are similar, the statistics of the counting rate, C_i, obtained by counting in a fixed time $\delta t_i > \sigma_{pi}$ is similar to the R_i statistics. By means of a discriminator it is possible to select only neutron detection pulses. All these processes have associated a transfer function $h_i(\omega)$.

The characteristic time δt_i produces a break frequency $\omega_{ci}/2\pi$ and as it was explained in section II.B, the disappearance of the detected neutrons produces a white noise with an amplitude $2R_i$. These processes explain the shape of the $^{(c)}G_{ii}$ in the high frequency region.

By measuring using an adequate band width BW (BW > $\omega_{ci}/2\pi$) it is possible to obtain:

$$f_i^{(c)} = \frac{\text{detection term of } {}^{(c)}G_{ii}(\alpha_1 \ll \omega \ll \omega_{ci})}{2\overline{C}_i} = \frac{\overline{R}_i}{\overline{C}_i} \quad \text{(A-1)}$$

If the detection device is working properly (without spurious counts), $f_i^{(c)}=1$.

In the current mode, there is an analogic integration with a characteristic detection time, τ_{ci}. This time constant depends on the detection devices (detector, amplifier and so on). This process, also has associated a detection transfer function $h_i(\omega)$ with a break frequency $\omega_{ci}(\tau_{ci})/2\pi$

The statistics of I_i depends on the statistics of R_i and q_i. The statistics of q_i, depends on the pressure an type of detector's gas, detector geometry (including wall efects), detector's voltage and type of particle detected. For this reason, in the normalized APSD ${}^{(I)}G_{ii}/(\overline{q_i})^2$, the detection term increases relatively to the ${}^{(c)}G_{ii}$ by the Bennett factor $B_i=\overline{q_i^2}/(\overline{q_i})^2$ (>1).

These results can also be obtained in another way. Following Difilippo (1987) the transformation of a sequence of ramdom events in time (input) into an analogous signal (output) through the action of a measuring device can drastically influence the statistics of the process under observation. The current I_i at time t is the superposition of the effects of events at earlier time t_n:

$$I_i(t) = \sum_{n=1}^{\infty} q_{n,i}\ f_i(t-t_n) \quad \text{(A-2)}$$

where $q_{n,i}$ is the charge generated at t_n in detector i and:

$$f_i(\tau) = \omega_{ci}\ e^{-\omega_{ci}\tau} \quad \text{(A-3)}$$

is assumed to be a good expression to represent the detection process in an IC, independent of t_n. Assuming also that the sequence of times t_n is distributed according to a Poisson distribution, using Eqs. (A-2) and (A-3), we obtained:

$$\overline{I}_i = \overline{q}_i . \overline{R}_i \quad \text{(A-4)}$$

and the APSD (using positive frequencies):

$$^{(I)}G_{ii} = 2\,\overline{R}_i\ \overline{q_i^2} \quad \text{(A-5)}$$

with the conditions $\alpha_1 \ll \omega$. and/or $\epsilon_i \ll (\bar{\beta})^2$ (A<<N in Eq. (**42**)).

By measurement (with an adequate BW) it is possible to obtain:

$$f_i^{(q)} = \frac{\text{detection term of } {}^{(I)}G_{ii}}{2\,\bar{I}_i} = \frac{{}^{(I)}G_{ii}(\alpha_i \ll \omega \ll \omega_{ci})}{2\,\bar{I}_i} \qquad \text{(A-6)}$$

if the detection device works properly (i.e. the Eq. (A-4) is valid):

$$f_i^{(q)} = \frac{\overline{q_i^2}}{\bar{q}_i} = \bar{q}_i + \frac{\sigma_{q_i}^2}{\bar{q}_i} > \bar{q}_i \qquad \text{(A-7)}$$

$f_i^{(q)}$ depends on charge statistics, i.e., a time constant value. Then it is possible to use $f_i^{(q)}$ in order to verify the properly functioning of a current detection device. The mean reasons that could modify $f_i^{(q)}$ are: high gamma detection, high and variable electric noise (i.e. rms value similar order than detection noise), high leakeage current (similar order than mean current) and IC's voltage outside of the plateau region. All these effects could affect $\bar{I}_i$ in a different way than ${}^{(I)}G_{ii}(\alpha_i \ll \omega \ll \omega_{ci})$ in Eq. (A-6)

APPENDIX B: Harmonics Contribution in a Compact Reactor.

In order to analyze the contribution of higher armonics in analytical APSD functions, data obtained from a theoretical model developed by Wentzeis et al (1988) was fitted using the first two terms of the modal expansion in Eq. (16). The reactor model considered is show in Fig. B-1.

The two group diffusion constants used in the calculations are shown in Table B-1.

The fitted function was:

$$F(\omega) = 10 \log \left[\frac{A_i^{(1)}}{\left(1+\frac{\omega^2}{\alpha_1^2}\right)} + \frac{A_i^{(2)}}{\left(1+\frac{\omega^2}{\alpha_2^2}\right)} \right] \tag{B-1}$$

where from Eqs. (17) to (20):

$$A_i^{(1)} = \frac{K}{\alpha_1} \left[a_i + b_i \right] \tag{B-2}$$

$$A_i^{(2)} = \frac{K}{\alpha_2} \left[b_i + c_i \right] \tag{B-3}$$

K: a normalization constant, and:

$$a_i = \frac{\langle\langle \chi_1^+(\vec{r})\chi_1^+(\vec{r}\,')\, G_{ss}(\vec{r},\vec{r}\,')\rangle\rangle \langle \Sigma_{di}\, \chi_1 \rangle^2}{2\alpha_1} \tag{B-4}$$

$$b_i = \frac{\langle\langle \chi_1^+(\vec{r})\chi_2^+(\vec{r}\,')\, G_{ss}(\vec{r},\vec{r}\,')\rangle\rangle \langle \Sigma_{di}\, \chi_1 \rangle \langle \Sigma_{di}\, \chi_2 \rangle}{(\alpha_1 + \alpha_2)} \tag{B-5}$$

$$c_i = \frac{\langle\langle \chi_2^+(\vec{r})\chi_2^+(\vec{r}\,')\, G_{ss}(\vec{r},\vec{r}\,')\rangle\rangle \langle \Sigma_{di}\, \chi_2 \rangle^2}{2\alpha_2} \tag{B-6}$$

The values obtained for the fitted parameters using Marquardt's method were:

$$\begin{cases} \dfrac{A_i^{(2)}}{A_i^{(1)}} = (1.12 \pm 0.23)\times 10^{-3} \\ \alpha_1 = (98.16 \pm 0.22)\ s^{-1} \\ \alpha_2 = (648 \pm 57)\ s^{-1} \end{cases} \tag{B-7}$$

From Eqs. (B-2), (B-3) and (B-7) and considering $0<c_i<<b_i$ (from Eq. (B-6)):

$$\frac{b_i}{(a_i+b_i)} < \frac{\alpha_2\, A_i^{(2)}}{\alpha_1\, A_i^{(1)}} = (7.4 \pm 1.6)\times10^{-3} \qquad \text{(B-8)}$$

These result shows that in the frequency region considered $\lambda_i<<\omega<\alpha_1$; $\alpha_2>>\alpha_1$ so it is possible to fit using the first term in Eq. (B-1). The contribution of armonics in the $A_i^{(1)}$ amplitude is lower than 0.9% but higher than the second term contribution. The second term contribution increase for greater ω and it is < 0.3% for $\omega=\alpha_1$.

LIST OF TABLES

Serie (s)	Control rod insertion(%↑)		Forced convection	Power range	Number of power steps	Calculus made in order to verify hyphotesis 1 and 2
	B3	B4				
1	45	100	NO	10 W to 5 Kw	9	$\overline{I_j}=a_j^{(s)}\overline{I_2}+b_j^{(s)}$ $\overline{P_{il}}=a_{il}^{(s)}\overline{I_2}+b_{il}^{(s)}$ $j=1,2,3$ $i,l=1,2$; $P\doteq\overline{\overline{P_{11}},\overline{P_{12}},\overline{P_{22}}}$ $P=m_i^{(s)}\overline{I_i}+n_i^{(s)}$ $i=1,2,3$
2	45	100	YES		9	
3	100	50	NO		9	
4	100	50	YES	5 Kw to 200 Kw	4	$\overline{I_N}=c^{(s)}\overline{I_3}+d^{(s)}$ P_{il}
5	45	100	YES		4	

(100%↑ means the rod is outside)

Table I

	$\overline{P_{i\ell}} = a_{i\ell}^{(s)}\overline{I_2} + b_{i\ell}^{(s)}$			
Serie (s)	$a_{11}^{(s)}$ [10^7 W/A]	$a_{12}^{(s)}$ [10^7 W/A]	$a_{22}^{(s)}$ [10^7 W/A]	$\alpha^{(s)}$ [1/s]
	$b_{11}^{(s)}$ [W]	$b_{12}^{(s)}$ [W]	$b_{22}^{(s)}$ [W]	
1	$7.16 \pm .08$	$7.07 \pm .06$	$7.16 \pm .05$	103.6 ± 1.2
	$2.42 \pm .72$	$0.86 \pm .17$	$0.48 \pm .18$	
2	$7.07 \pm .15$	$7.06 \pm .10$	$7.19 \pm .14$	101.4 ± 1.0
	$-0.42 \pm .41$	$-0.04 \pm .52$	$0.11 \pm .27$	
3	$7.94 \pm .08$	$7.74 \pm .06$	$7.94 \pm .07$	$102.8 \pm .9$
	$2.41 \pm .32$	$1.62 \pm .13$	$0.50 \pm .19$	

Table II

Serie (s)	$P = m_i^{(s)} \overline{I}_i + n_i^{(s)}$			$\overline{I}_N = c^{(s)} \overline{I}_3 + d^{(s)}$	$\frac{m^{(s)}}{c^{(s)}}$ $[10^{14} W/A]$
	$m_1^{(s)}$ $[10^7 W/A]$ / $n_1^{(s)}$ $[W]$	$m_2^{(s)}$ $[10^7 W/A]$ / $n_2^{(s)}$ $[W]$	$m_3^{(s)}$ $[10^7 W/A]$ / $n_3^{(s)}$ $[W]$	$c^{(s)}$ $[10^{-5}]$ / $d^{(s)}$ $[10^{-12} A]$	
1	7.38 ± .08	7.13 ± .07	372 ± 3		
	0.48 ± .43	0.96 ± .38	1.01 ± .33		
2	7.47 ± .09	7.12 ± .11	376 ± 7		
	-0.63 ± .32	-0.13 ± .44	-0.89 ± .57		
3	7.16 ± .03	7.86 ± .07	328 ± 3		
	-.003 ± .16	1.58 ± .32	-1.18 ± .41		
4				1.161 ± .023	2.825 ± .063
				6.9 ± 5.9	
5				1.338 ± .003	2.785 ± .056
				2.51 ± .26	
					2.803 ± .042

Table III

CONSTANT	CORE	WATER	GRAPHITE
Σ_{1a} [cm^{-1}]	1.9281×10^{-3}	4.5966×10^{-4}	1.1133×10^{-4}
Σ_{12} [cm^{-1}]	3.1879×10^{-2}	4.8200×10^{-2}	5.1563×10^{-3}
Σ_{2a} [cm^{-1}]	6.1013×10^{-2}	1.7034×10^{-2}	2.9596×10^{-3}
D_1 [cm]	1.4218	1.1906	1.3446
D_2 [cm]	0.2248	0.1722	0.7064
$\nu\Sigma_f$ [cm^{-1}]	8.8048×10^{-2}		

$\bar{v}_1 = 5 \times 10^7$ cm/s $\quad\quad$ $\bar{v}_2 = 2.2 \times 10^5$ cm/s

Table B-1

LIST OF FIGURES:

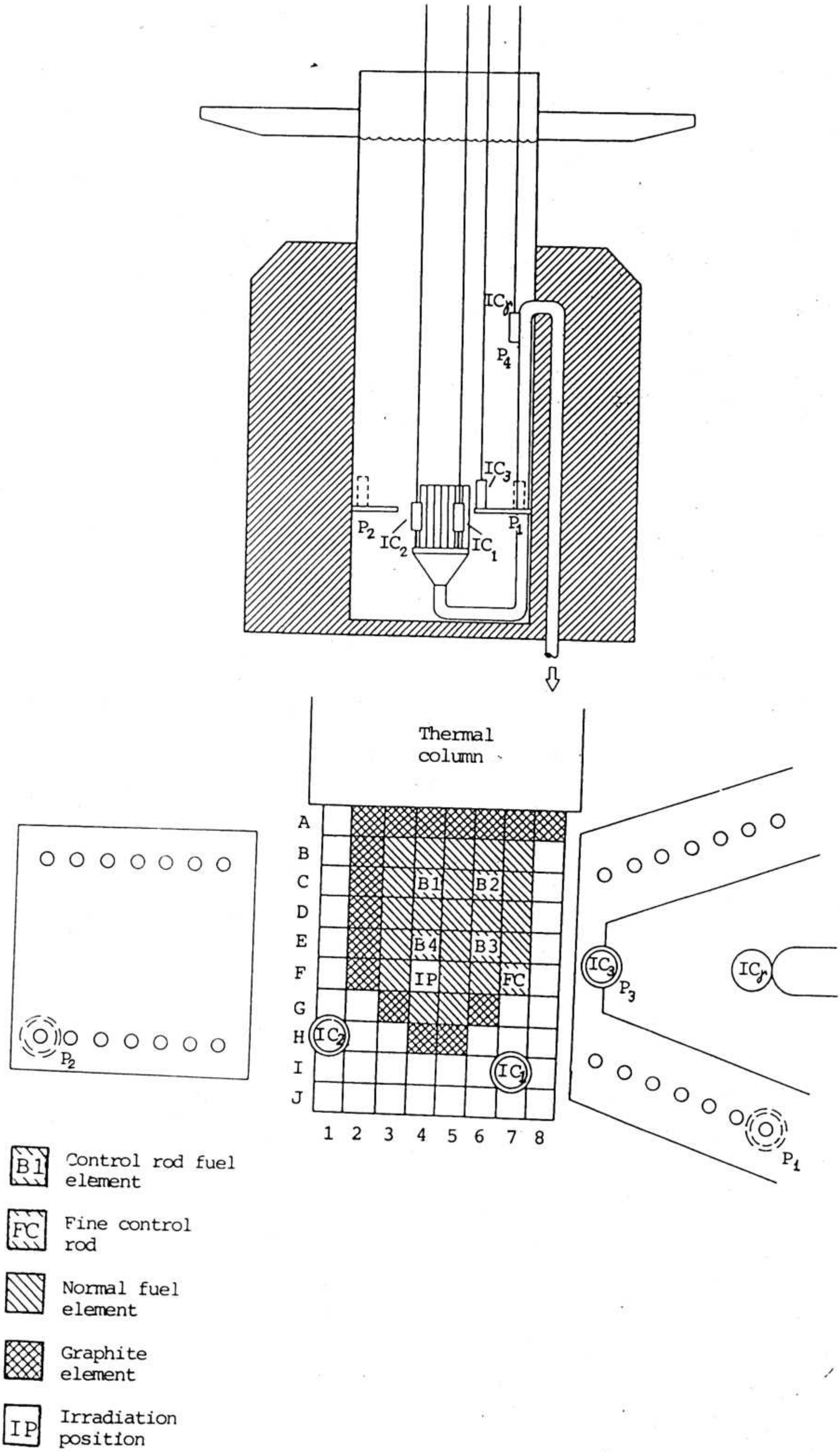
IC$_\gamma$
P$_4$
IC$_3$
P$_2$
IC$_2$
IC$_1$
P$_1$
Thermal column
A
B
C
D
E
F
G
H
I
J
1 2 3 4 5 6 7 8
B1
B2
B4
B3
IP
FC
IC$_2$
IC$_1$
IC$_3$
P$_3$
IC$_\gamma$
P$_2$
P$_1$
B1 Control rod fuel element
FC Fine control rod
Normal fuel element
Graphite element
IP Irradiation position

Fig. 1

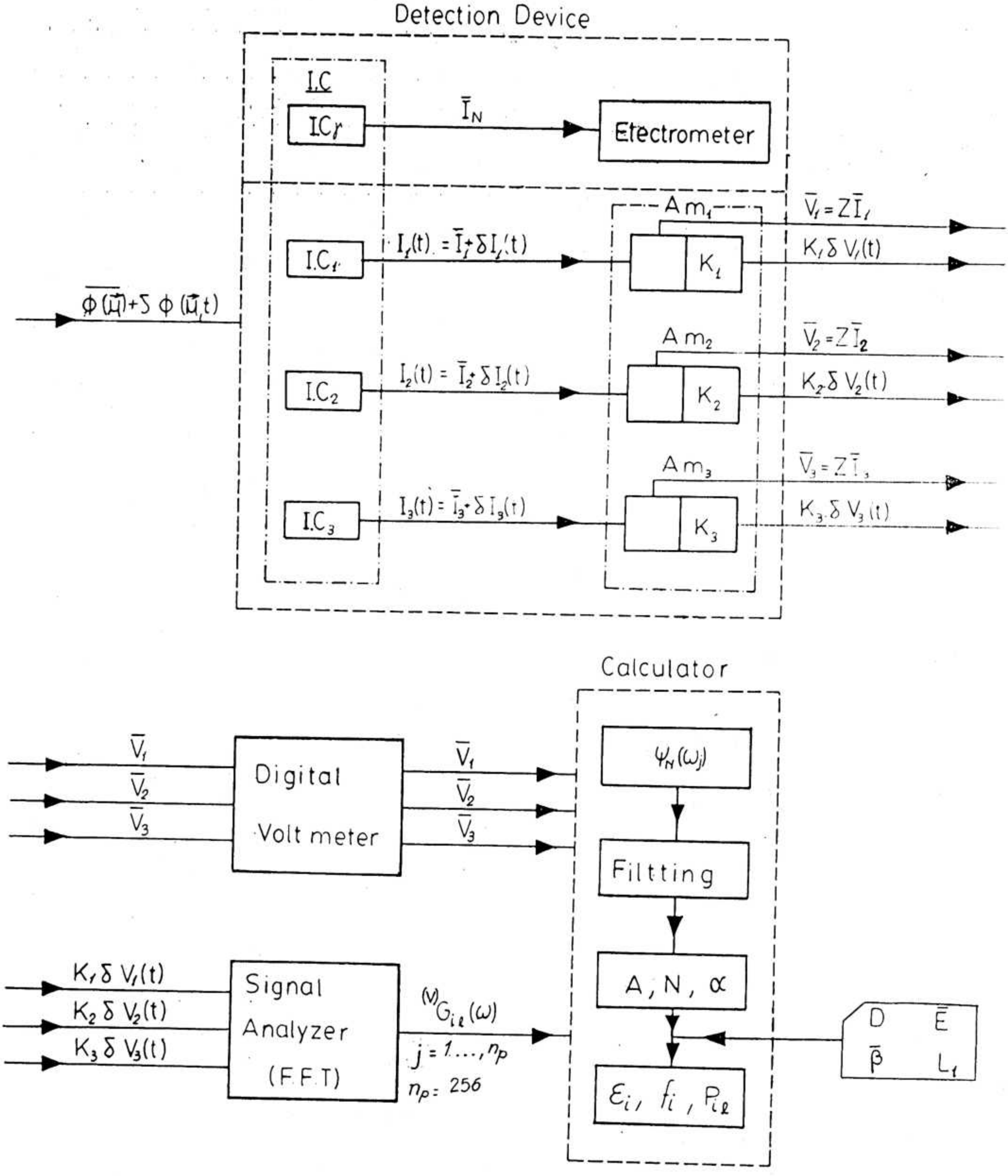
Detection Device
I.C
ICr
$\bar{I}_N$
Electrometer
$\overline{\Phi(\vec{u})} + \delta\,\Phi(\vec{u},t)$
I.C1
$I_1(t) = \bar{I}_1 + \delta I_1(t)$
Am1
K1
$\bar{V}_1 = Z\bar{I}_1$
$K_1\,\delta V_1(t)$
I.C2
$I_2(t) = \bar{I}_2 + \delta I_2(t)$
Am2
K2
$\bar{V}_2 = Z\bar{I}_2$
$K_2\,\delta V_2(t)$
I.C3
$I_3(t) = \bar{I}_3 + \delta I_3(t)$
Am3
K3
$\bar{V}_3 = Z\bar{I}_3$
$K_3\,\delta V_3(t)$
Calculator
$\bar{V}_1$
$\bar{V}_2$
$\bar{V}_3$
Digital
Volt meter
$\psi_N(\omega_j)$
Filtting
A, N, α
$K_1\,\delta V_1(t)$
$K_2\,\delta V_2(t)$
$K_3\,\delta V_3(t)$
Signal
Analyzer
(F.F.T)
${}^{(V)}G_{il}(\omega)$
$j = 1\ldots, n_p$
$n_p = 256$
D
$\bar{E}$
$\bar{\beta}$
L_1
$\varepsilon_i,\ f_i,\ P_{il}$

Fig. 2

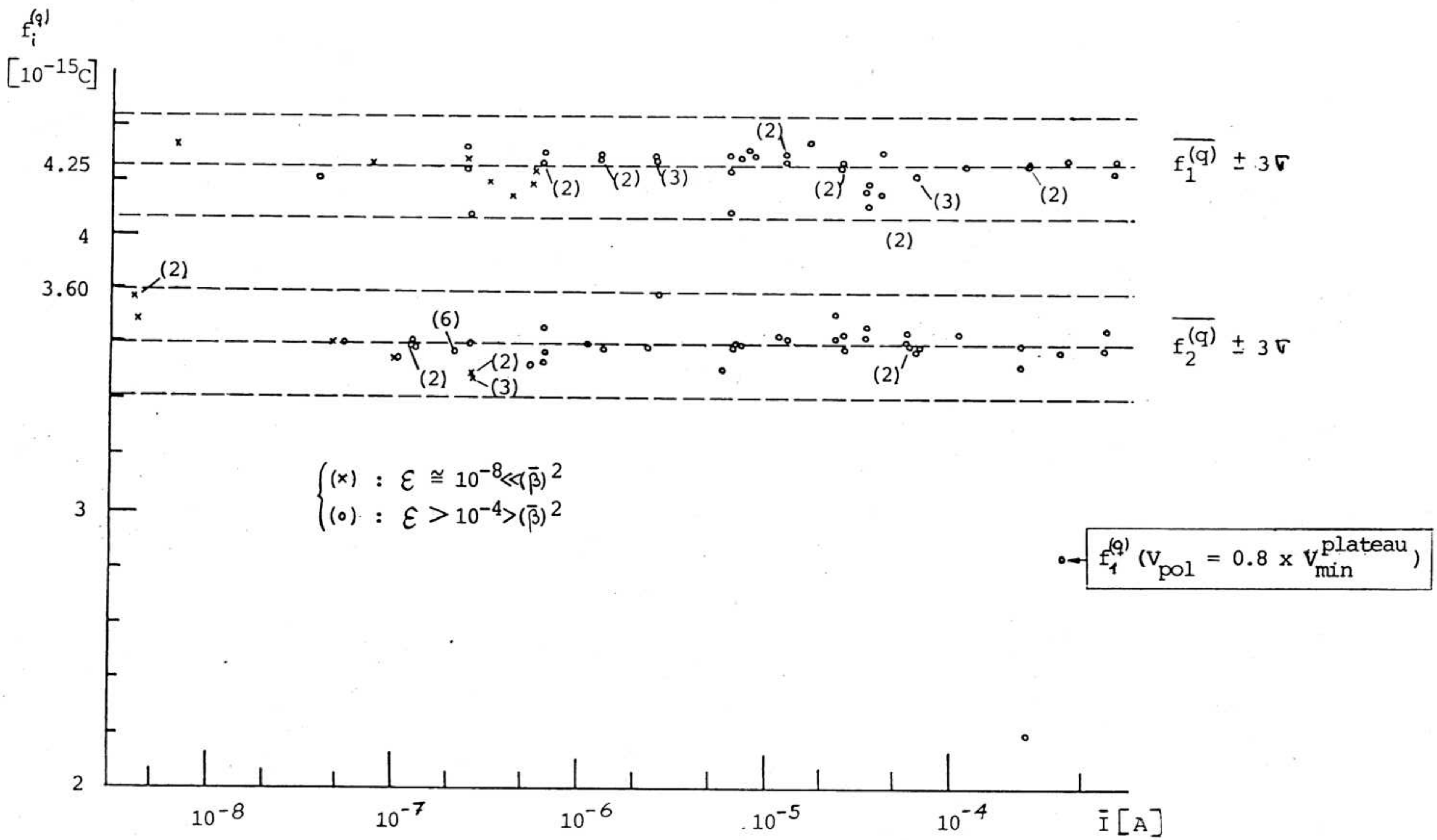
$f_i^{(q)}$
$[10^{-15}C]$
4.25
4
3.60
3
2
10^{-8}
10^{-7}
10^{-6}
10^{-5}
10^{-4}
$\bar{I}$ [A]
$\overline{f_1^{(q)}} \pm 3\sigma$
$\overline{f_2^{(q)}} \pm 3\sigma$
(x) : $\varepsilon \cong 10^{-8} \ll (\bar{\beta})^2$
(o) : $\varepsilon > 10^{-4} > (\bar{\beta})^2$
$f_1^{(q)}$ ($V_{pol} = 0.8 \times V_{min}^{plateau}$)
(2)
(3)
(6)

Fig 3

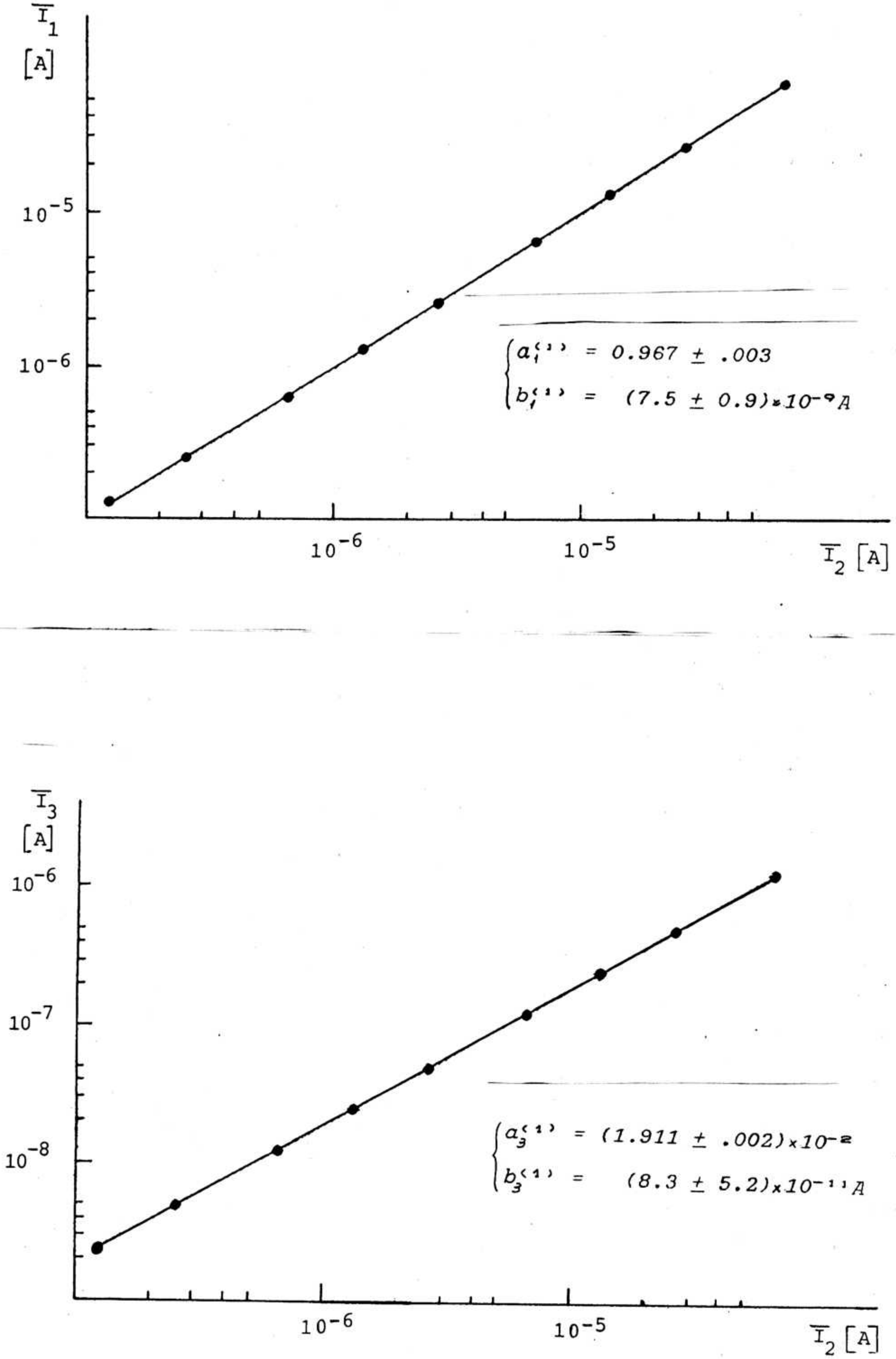
$\overline{I}_1$ [A]
10^{-5}
10^{-6}
$a_1^{(1)} = 0.967 \pm .003$
$b_1^{(1)} = (7.5 \pm 0.9)\times 10^{-9}$ A
10^{-6}
10^{-5}
$\overline{I}_2$ [A]
$\overline{I}_3$ [A]
10^{-6}
10^{-7}
10^{-8}
$a_3^{(1)} = (1.911 \pm .002)\times 10^{-2}$
$b_3^{(1)} = (8.3 \pm 5.2)\times 10^{-11}$ A
10^{-6}
10^{-5}
$\overline{I}_2$ [A]

Fig. 4

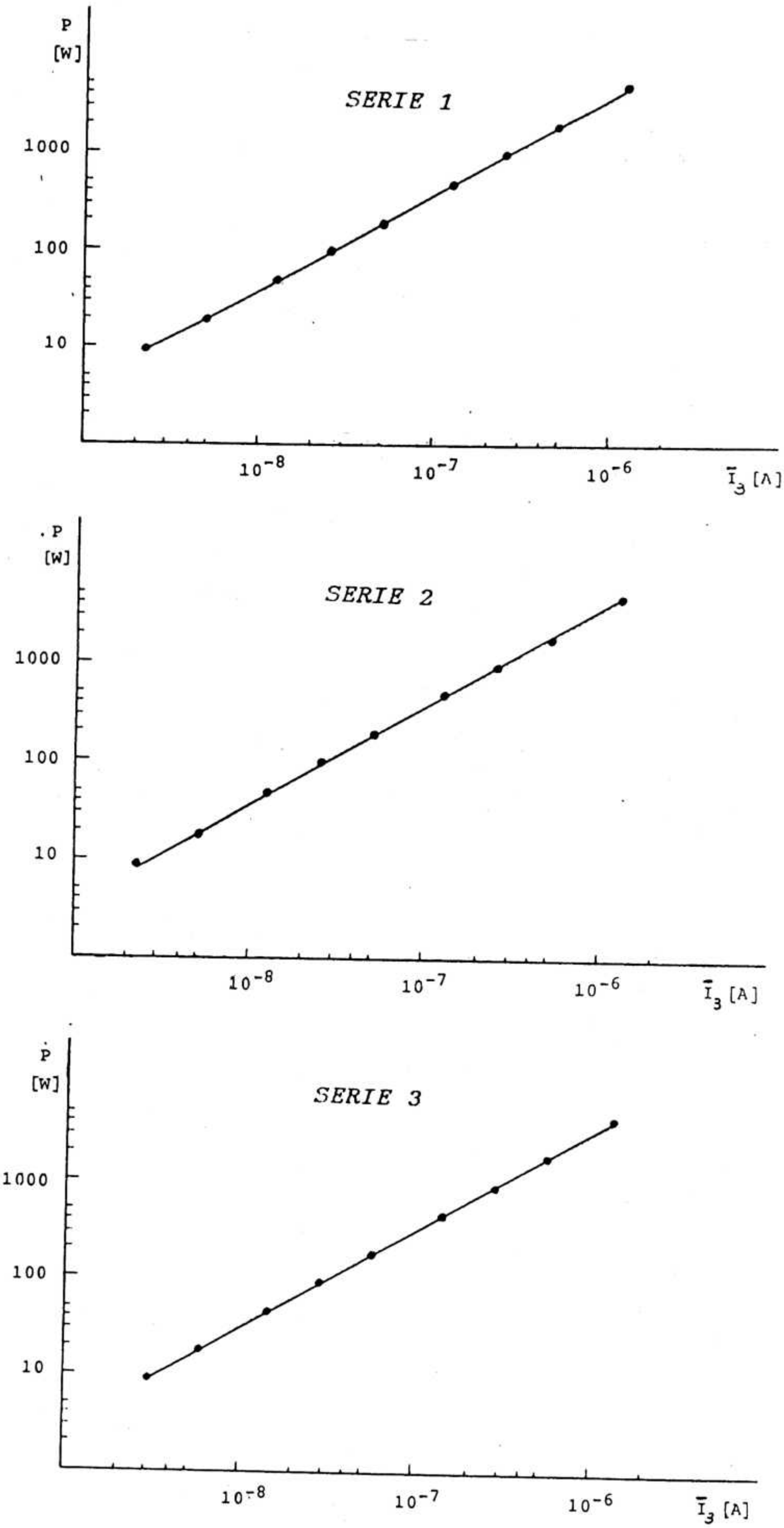
P
[W]
SERIE 1
1000
100
10
10^{-8}
10^{-7}
10^{-6}
$\bar{I}_3$ [A]
P
[W]
SERIE 2
1000
100
10
10^{-8}
10^{-7}
10^{-6}
$\bar{I}_3$ [A]
P
[W]
SERIE 3
1000
100
10
10^{-8}
10^{-7}
10^{-6}
$\bar{I}_3$ [A]

Fig. 5

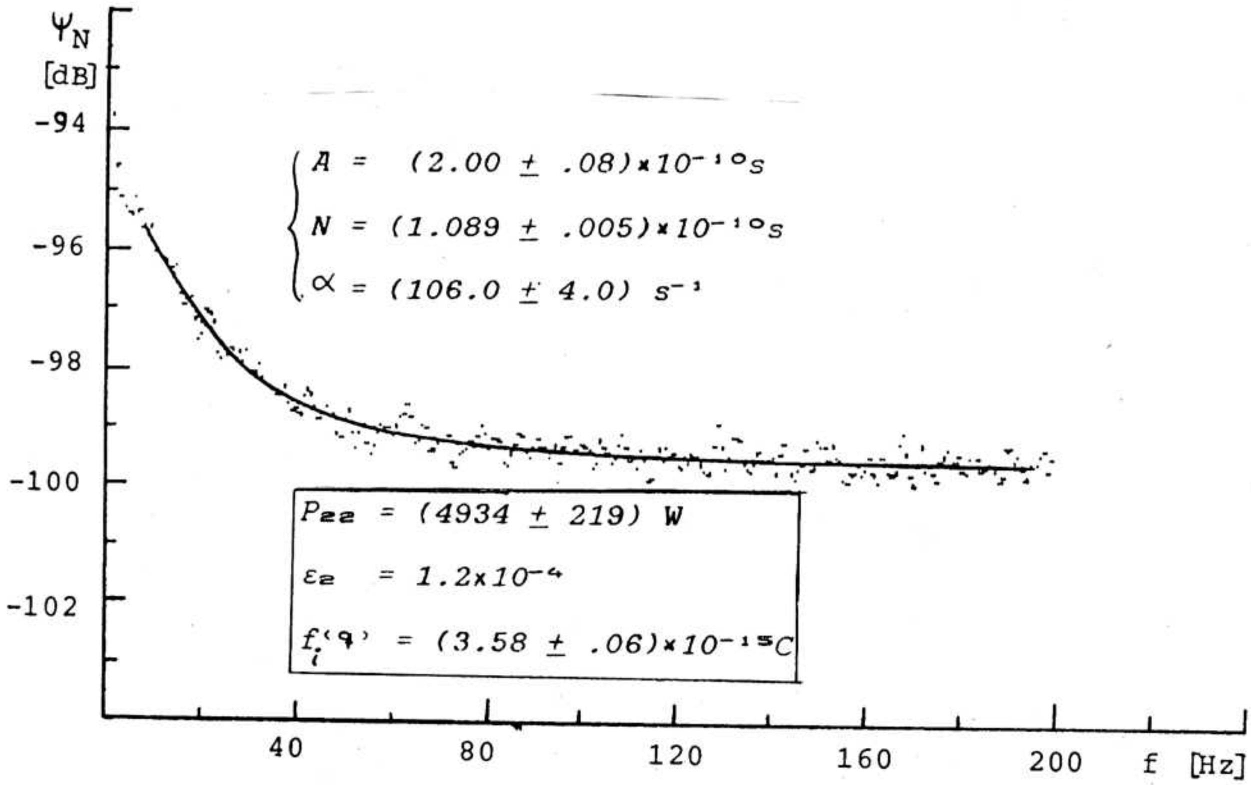

Ψ_N
[dB]
-94
-96
-98
-100
-102
$A = (2.00 \pm .08)\times10^{-10}s$
$N = (1.089 \pm .005)\times10^{-10}s$
$\alpha = (106.0 \pm 4.0)\ s^{-1}$
$P_{22} = (4934 \pm 219)$ W
$\varepsilon_2 = 1.2\times10^{-4}$
$f_i^{(q)} = (3.58 \pm .06)\times10^{-15}C$
40
80
120
160
200
f [Hz]

Fig. 6

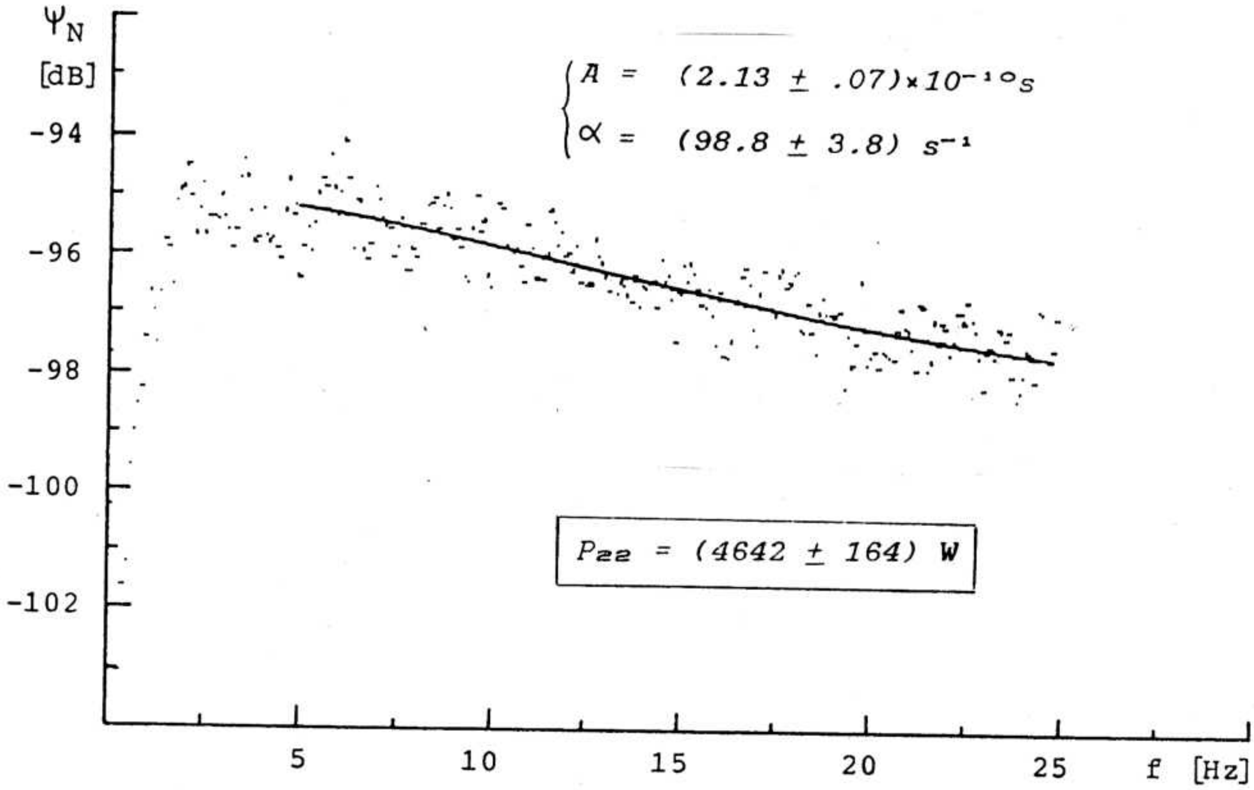

Ψ_N
[dB]
-94
-96
-98
-100
-102
$A = (2.13 \pm .07)\times10^{-10}s$
$\alpha = (98.8 \pm 3.8)\ s^{-1}$
$P_{22} = (4642 \pm 164)$ W
5
10
15
20
25
f [Hz]

Fig. 7

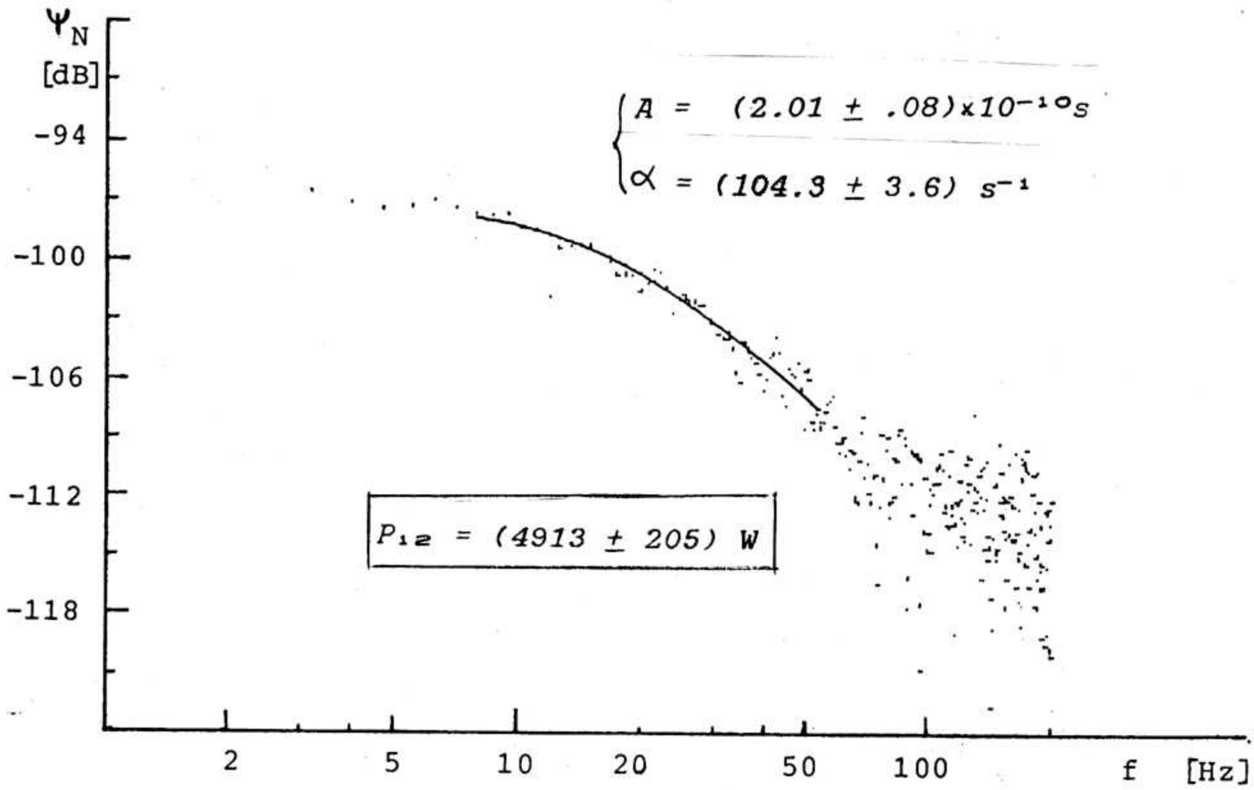

Ψ_N [dB]
-94
-100
-106
-112
-118
$A = (2.01 \pm .08) \times 10^{-10}$ s
$\alpha = (104.3 \pm 3.6)$ s^{-1}
$P_{12} = (4913 \pm 205)$ W
2
5
10
20
50
100
f [Hz]

Fig. 8

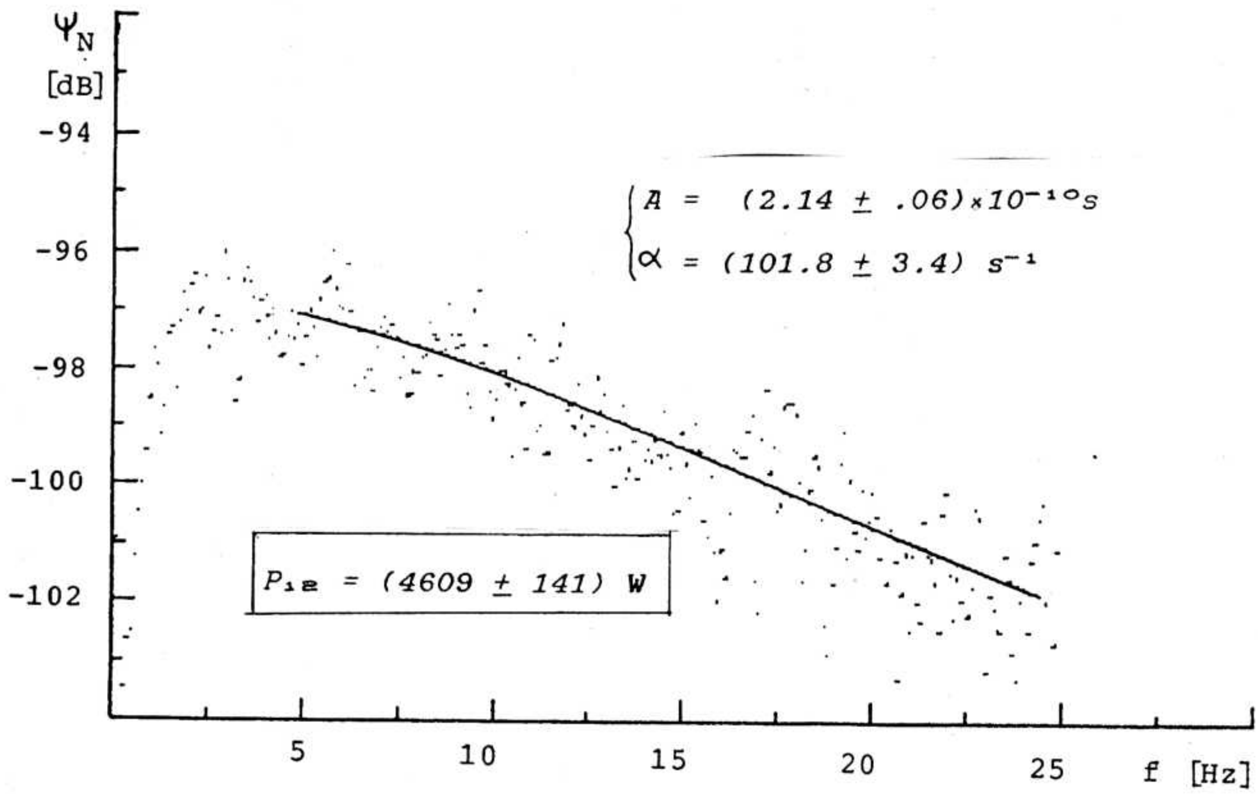

Ψ_N [dB]
-94
-96
-98
-100
-102
$A = (2.14 \pm .06) \times 10^{-10}$ s
$\alpha = (101.8 \pm 3.4)$ s^{-1}
$P_{12} = (4609 \pm 141)$ W
5
10
15
20
25
f [Hz]

Fig. 9

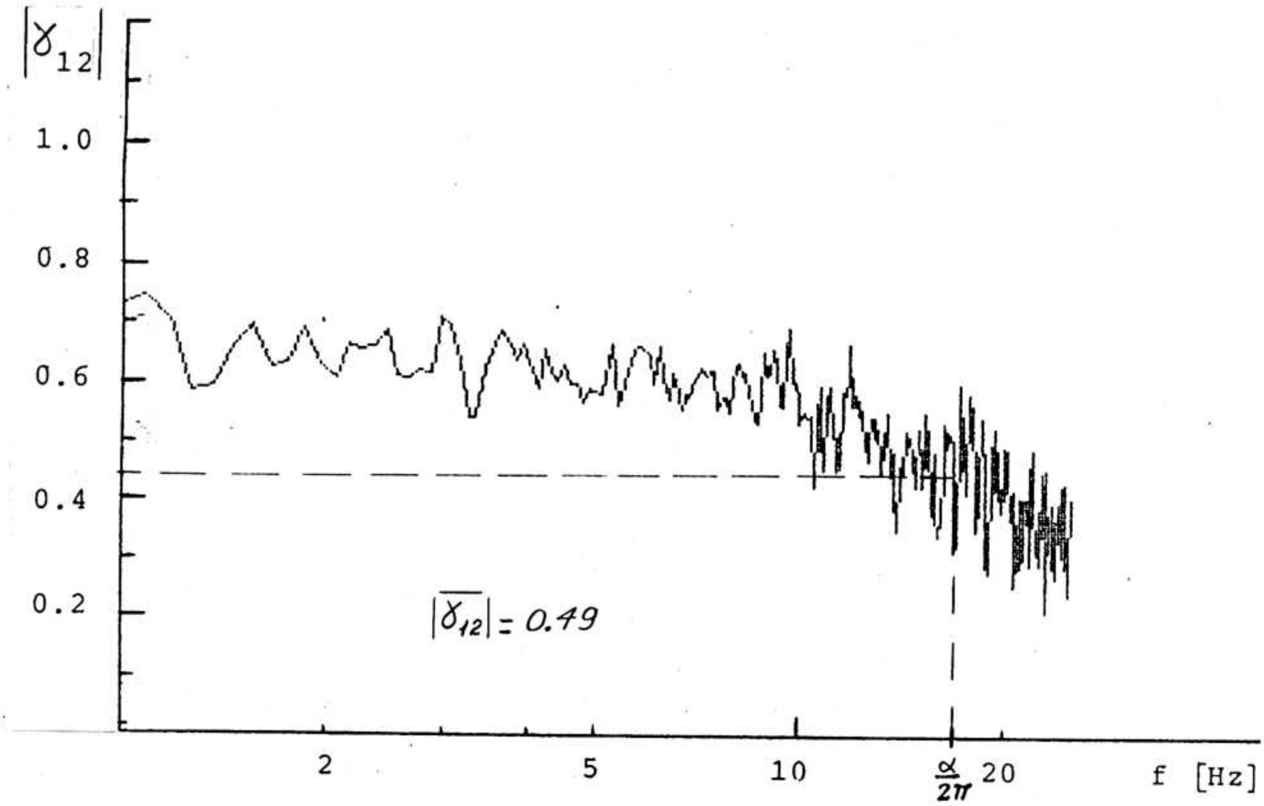

$|\gamma_{12}|$
1.0
0.8
0.6
0.4
0.2
$|\overline{\gamma_{12}}| = 0.49$
2
5
10
$\frac{\alpha}{2\pi}$
20
f [Hz]

Fig. 10

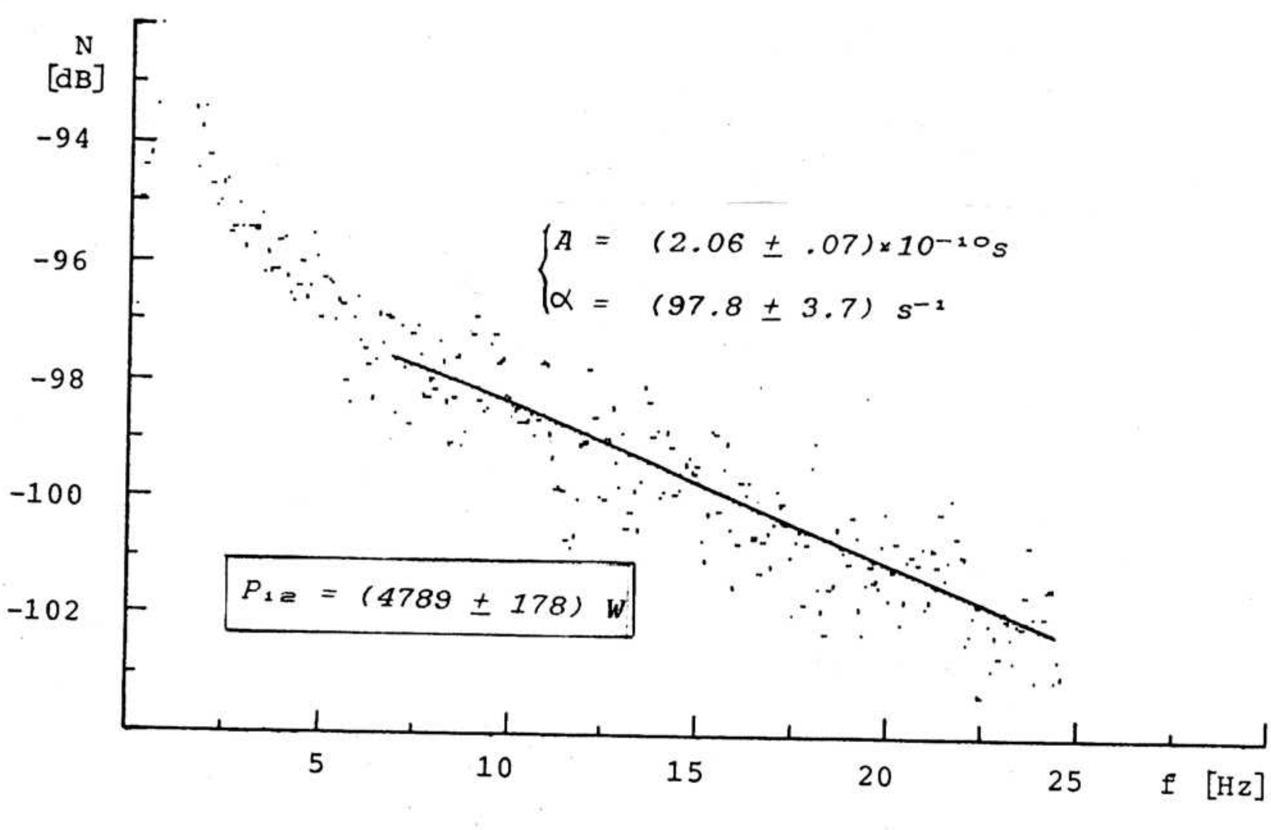

N [dB]
-94
-96
-98
-100
-102
$A = (2.06 \pm .07) \times 10^{-10} s$
$\alpha = (97.8 \pm 3.7)\ s^{-1}$
$P_{12} = (4789 \pm 178)\ W$
5
10
15
20
25
f [Hz]

Fig. 11

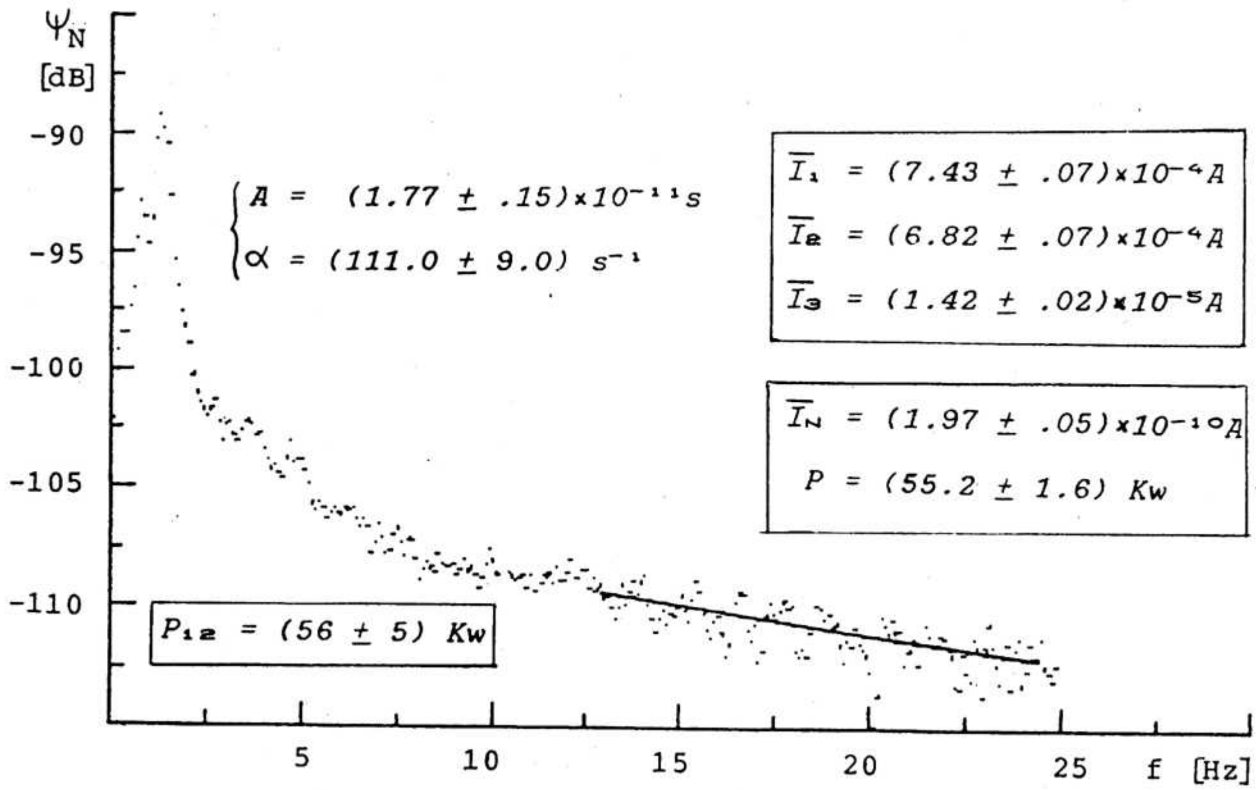

Ψ_N
[dB]
-90
-95
-100
-105
-110
$A = (1.77 \pm .15) \times 10^{-11} s$
$\alpha = (111.0 \pm 9.0)\ s^{-1}$
$\overline{I}_1 = (7.43 \pm .07) \times 10^{-4} A$
$\overline{I}_2 = (6.82 \pm .07) \times 10^{-4} A$
$\overline{I}_3 = (1.42 \pm .02) \times 10^{-5} A$
$\overline{I}_N = (1.97 \pm .05) \times 10^{-10} A$
$P = (55.2 \pm 1.6)$ Kw
$P_{12} = (56 \pm 5)$ Kw
5
10
15
20
25
f [Hz]

Fig. 12

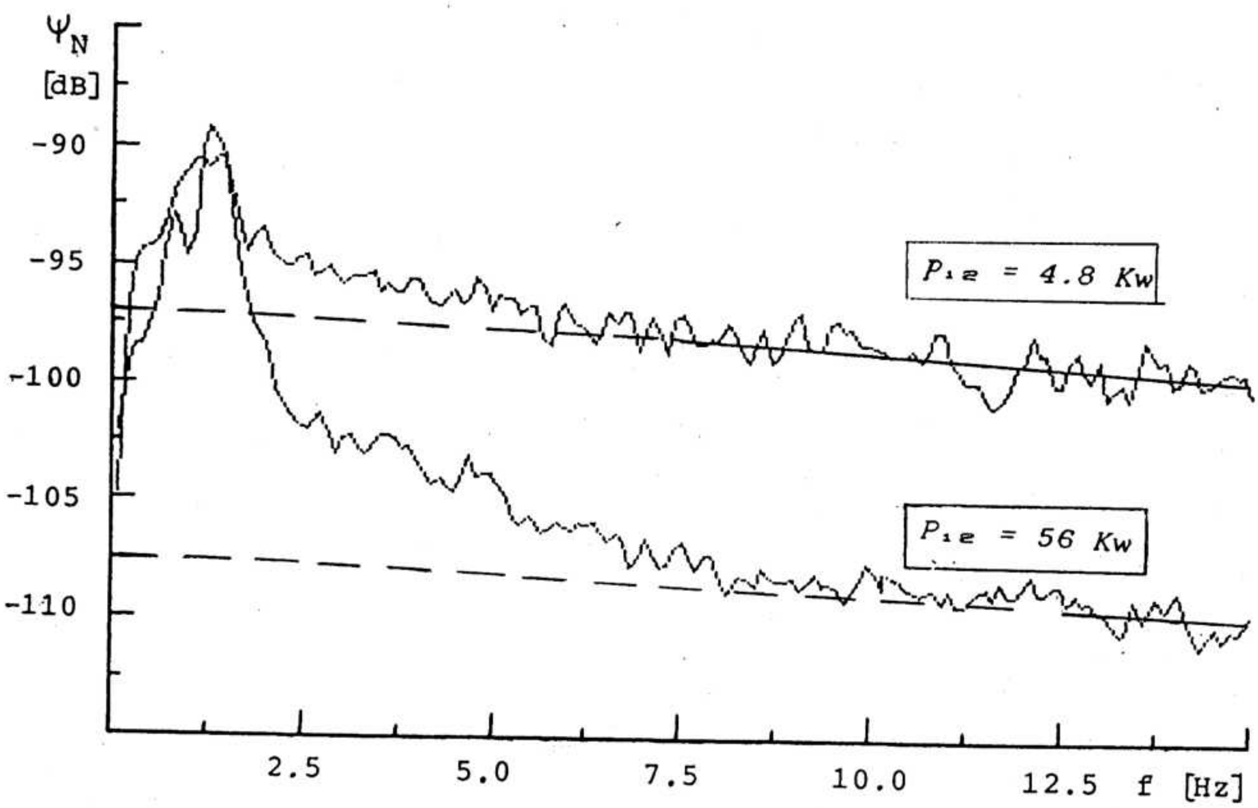

Ψ_N
[dB]
-90
-95
-100
-105
-110
$P_{12} = 4.8$ Kw
$P_{12} = 56$ Kw
2.5
5.0
7.5
10.0
12.5
f [Hz]

Fig. 13

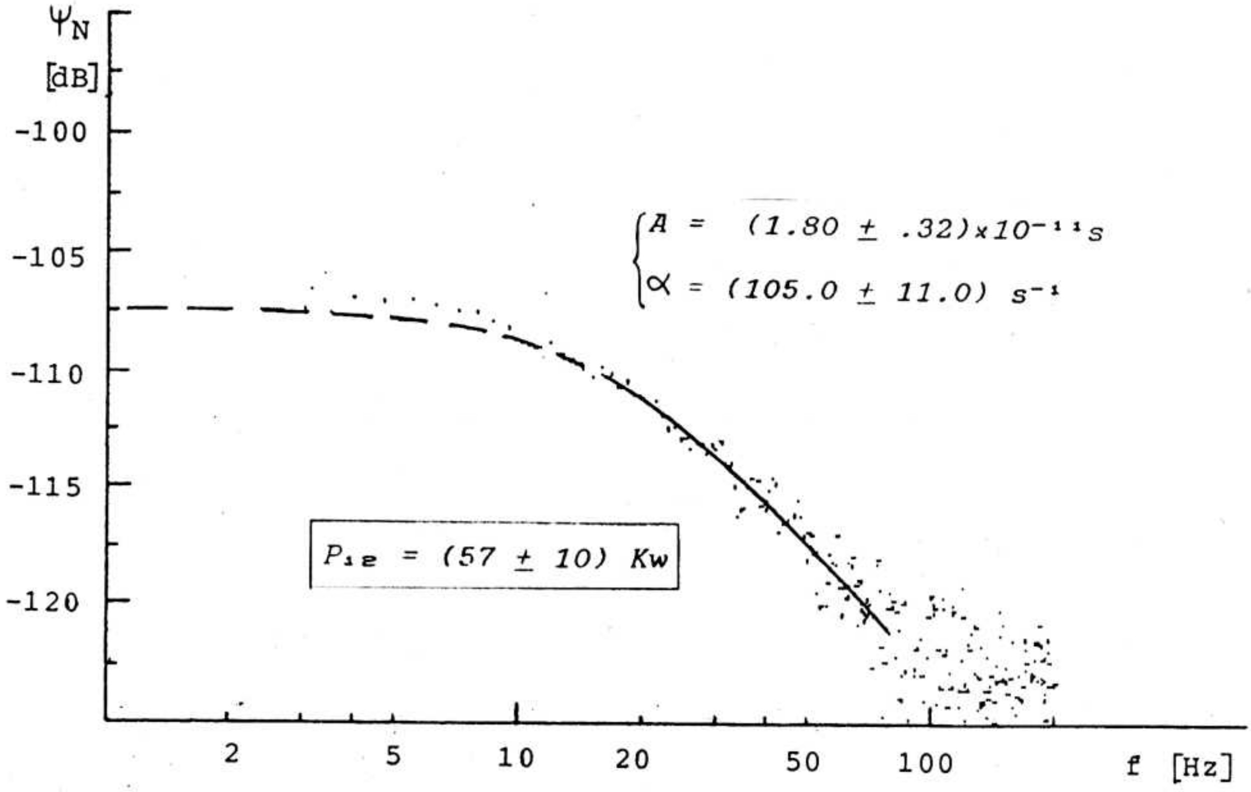

Ψ_N
[dB]
-100
-105
-110
-115
-120
$A = (1.80 \pm .32) \times 10^{-11} s$
$\alpha = (105.0 \pm 11.0)\ s^{-1}$
$P_{12} = (57 \pm 10)$ Kw
2
5
10
20
50
100
f [Hz]

Fig. 14

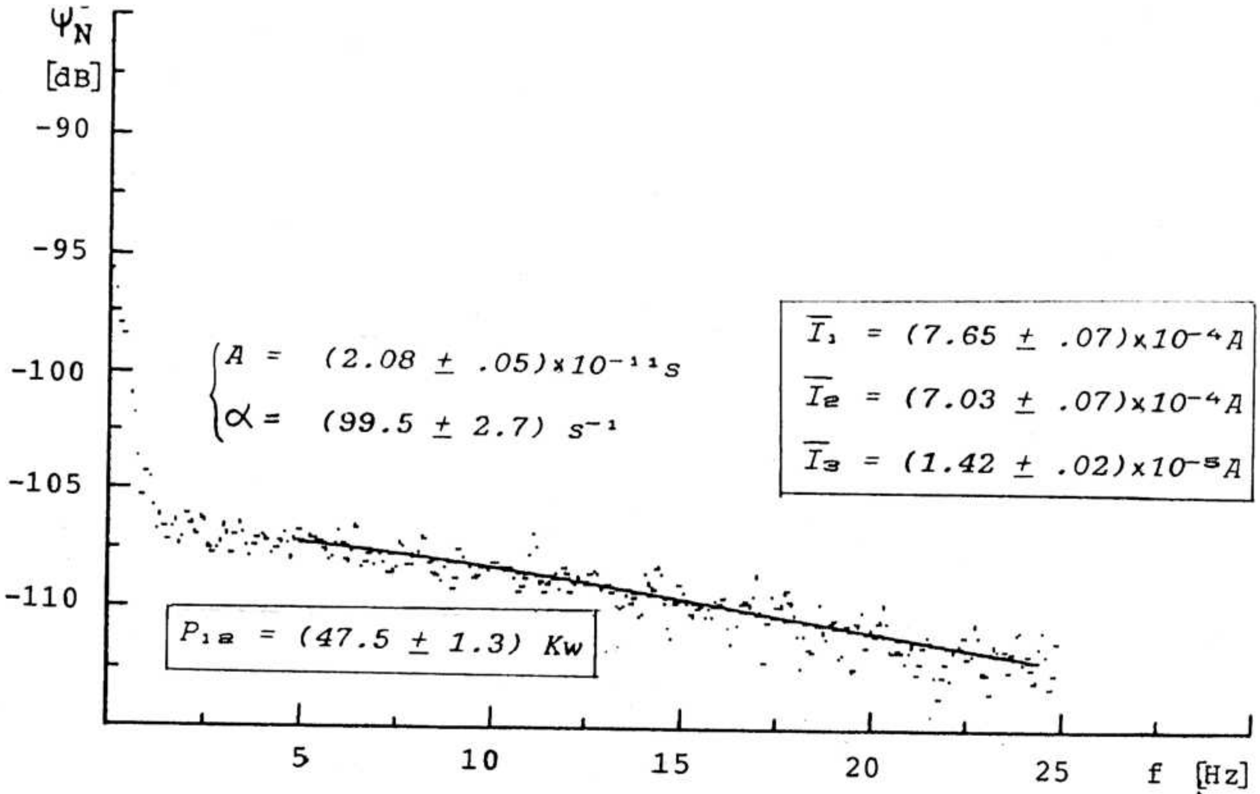

Ψ_N^-
[dB]
-90
-95
-100
-105
-110
$A = (2.08 \pm .05) \times 10^{-11} s$
$\alpha = (99.5 \pm 2.7)\ s^{-1}$
$\overline{I}_1 = (7.65 \pm .07) \times 10^{-4} A$
$\overline{I}_2 = (7.03 \pm .07) \times 10^{-4} A$
$\overline{I}_3 = (1.42 \pm .02) \times 10^{-5} A$
$P_{12} = (47.5 \pm 1.3)$ Kw
5
10
15
20
25
f [Hz]

Fig. 15

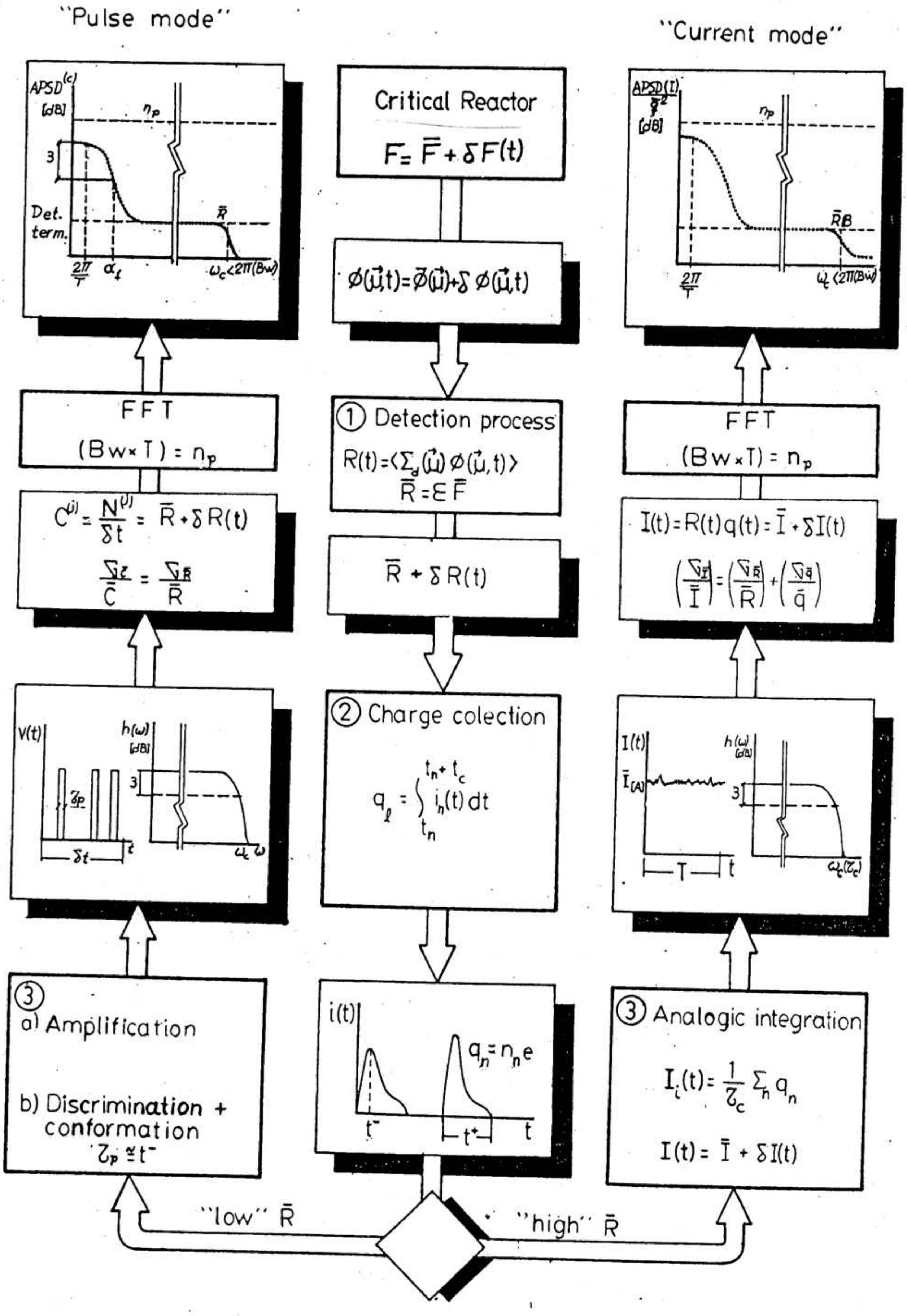
"Pulse mode"
"Current mode"
Critical Reactor
F= F̄ + δF(t)
φ(μ⃗,t)=φ̄(μ⃗)+δφ(μ⃗,t)
① Detection process
R(t)=⟨Σd(μ⃗) φ(μ⃗,t)⟩
R̄ = ε F̄
R̄ + δR(t)
② Charge colection
FFT
(Bw×T) = np
FFT
(Bw×T) = np
③
a) Amplification
b) Discrimination + conformation
τp ≅ t⁻
③ Analogic integration
I(t) = Ī + δI(t)
"low" R̄
"high" R̄
Det. term.

Fig. A-1

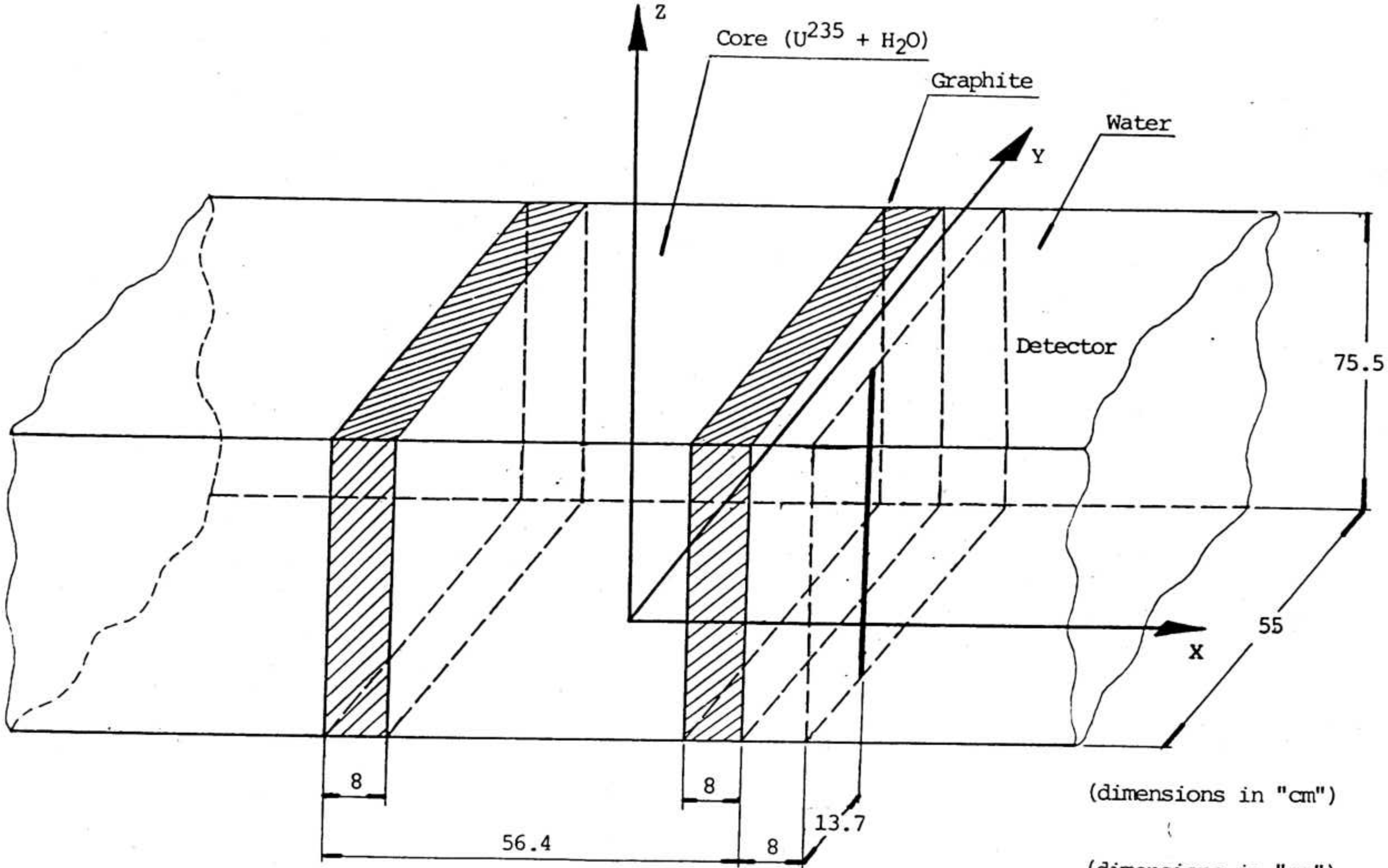

$$\begin{cases} \bar{\beta} = 0.0078 \\ \dfrac{\bar{\beta}}{\Lambda} = 98.34\ S^{-1} \end{cases}$$

(dimensions in "cm")

(dimensions in "cm")

Fig. B- 1